

# VTEM™ Plus

## REPORT ON A HELICOPTER-BORNE VERSATILE TIME DOMAIN ELECTROMAGNETIC (VTEM™ Plus) AND HORIZONTAL MAGNETIC GRADIOMETER GEOPHYSICAL SURVEY

| | |
|---|---|
| PROJECT: | BAYHORSE IDAHO/OREGON GEOPHYSICS PROJECT |
| LOCATION: | HUNTINGTON, OREGON & WEISER, IDAHO |
| FOR: | BAYHORSE SILVER INC. |
| SURVEY FLOWN: | JANUARY 2024 |
| PROJECT: | GL230249 |

Geotech Ltd.
270 Industrial Parkway South
Aurora, ON Canada L4G 3T9

Tel: +1 905 841 5004
Web: www.geotech.ca
Email: info@geotech.ca

GEOTECH
AIRBORNE GEOPHYSICAL SURVEYS

# TABLE OF CONTENTS

EXECUTIVE SUMMARY ..... III
1. INTRODUCTION ..... 1
1.1 General Considerations ..... 1
1.2 Survey And System Specifications ..... 2
1.3 Topographic Relief And Cultural Features ..... 3
2. DATA ACQUISITION ..... 4
2.1 Survey Area ..... 4
2.2 Survey Operations ..... 4
2.3 Flight Specifications ..... 4
2.4 Aircraft and Equipment ..... 5
2.4.1 Survey Aircraft ..... 5
2.4.2 Electromagnetic System ..... 5
2.4.3 Full Waveform VTEM™ Sensor Calibration ..... 9
2.4.4 Horizontal Magnetic Gradiometer ..... 9
2.4.5 Radar Altimeter ..... 9
2.4.6 GPS Navigation System ..... 9
2.4.7 Digital Acquisition System ..... 10
2.5 Base Station ..... 10
3. PERSONNEL ..... 11
4. DATA PROCESSING AND PRESENTATION ..... 12
4.1 Flight Path ..... 12
4.2 Electromagnetic Data ..... 12
4.3 Horizontal Magnetic Gradiometer Data ..... 14
4.4 Tau Parameter And CVG ..... 15
5. DELIVERABLES ..... 16
5.1 Survey Report ..... 16
5.2 Maps ..... 16
5.3 Digital Data ..... 17
6. CONCLUSIONS AND RECOMMENDATIONS ..... 21

# LIST OF FIGURES

Figure 1: Survey location ..... 1
Figure 2: Survey area location on Google Earth. ..... 2
Figure 3: Flight path over a Google Earth Image. ..... 3
Figure 4: VTEM™ Transmitter Current Waveform ..... 5
Figure 5: VTEM™plus System Configuration. ..... 8
Figure 6: X, Fraser filtered X and Z components for a "thin" sub-vertical conductor. ..... 13

# LIST OF TABLES

Table 1: Survey Specifications ..... 4
Table 2: Survey Schedule ..... 4
Table 3: Off-Time Decay Sampling Scheme ..... 6
Table 4: VTEM™ System Specifications ..... 8
Table 5: Acquisition Sampling Rates ..... 10
Table 6: Geosoft GDB Data Format ..... 17
Table 7: Geosoft Resistivity Depth Image GDB Data Format ..... 19
Table 8: Geosoft database for the VTEM waveform ..... 20

# APPENDICES

A. Survey Location Map ..... A1
B. Survey Area Coordinates ..... B1
C. Geophysical Maps ..... C1
D. Generalized Modelling Results of the VTEM System ..... D1
E. TAU Analysis ..... E1
F. TEM Resistivity Depth Imaging (RDI) ..... F1
G. Resistivity Depth Images (RDI) ..... G1

# EXECUTIVE SUMMARY

## BAYHORSE IDAHO/OREGON GEOPHYSICS PROJECT
## Huntington, Oregon & Weiser, Idaho

During January 5th to January 17th, 2024, Geotech Ltd. carried out a helicopter-borne geophysical survey for Bayhorse Silver Inc. over the Bayhorse Idaho/Oregon Geophysics Project, situated near Huntington, Oregon & Weiser, Idaho.

Principal geophysical sensors included a versatile time domain electromagnetic (VTEM™ Plus) system and a horizontal magnetic gradiometer with two caesium sensors. Ancillary equipment included a GPS navigation system and a radar altimeter. A total of 78 line-kilometres of geophysical data were acquired during the survey.

In-field data quality assurance and preliminary processing were carried out on a daily basis during the acquisition phase. Preliminary and final data processing, including generation of final digital data and map products were undertaken from the office of Geotech Ltd. in Aurora, Ontario.

The processed survey results are presented as the following maps:

- Electromagnetic stacked profiles of the B-field Z Component,
- Electromagnetic stacked profiles of dB/dt Z Components,
- B-Field Z Component Channel grid,
- dB/dt Z Component Channel grid,
- dB/dt X Component Fraser Filtered Channel grid,
- Total Magnetic Intensity (TMI),
- Calculated Vertical Gradient (CVG) of Total Magnetic Intensity (TMI),
- Magnetic Total Horizontal Gradient (TotHG),
- Magnetic Tilt-Angle Derivative (TiltDrv),
- Power Line Monitor (PLM),
- Calculated Time Constant (Tau) with Calculated Magnetic Vertical Derivative contours,
- Resistivity Depth Images (RDI) sections and depth slices are presented (pdf format).

Digital data includes all electromagnetic and magnetic products, plus ancillary data including the waveform.

The survey report describes the procedures for data acquisition, equipment used, processing, final image presentation and the specifications for the digital data set.

# 1. INTRODUCTION

## 1.1 GENERAL CONSIDERATIONS

Geotech Ltd. performed a helicopter-borne geophysical survey for Bayhorse Silver Inc. over the Bayhorse Idaho/Oregon Geophysics Project situated near Huntington, Oregon & Weiser, Idaho (Figure 1).

Graeme O'Neill represented Bayhorse Silver Inc. during the data acquisition and data processing phases of this project.

The geophysical surveys consisted of helicopter borne EM using the versatile time-domain electromagnetic (VTEM™) plus system with Full-Waveform processing. Measurements consisted of Vertical (Z), In-line(X), and Cross-line Horizontal (Y) components of the EM fields using an induction coil, and a horizontal magnetic gradiometer using two caesium magnetometers. A total of 78 line-km of geophysical data were acquired during the survey.

The crew was based out of Baker City (Figure 2) in Oregon for the acquisition phase of the survey. Survey flying started on January 15th and was completed on January 16th, 2024.

Data quality control and quality assurance, and preliminary data processing were carried out on a daily basis during the acquisition phase of the project. Final data processing followed immediately after the end of the survey. Final reporting, data presentation and archiving were completed from the Aurora office of Geotech Ltd. in January 2024.




Figure 1: Survey location

## 1.2 SURVEY AND SYSTEM SPECIFICATIONS

The Bayhorse Idaho/Oregon Geophysics Project survey area is located approximately 12 kilometres northeast of Huntington and 60 kilometres southeast of Baker City, Oregon and approximately 30 km northwest of Weiser, Idaho (Figure 2).




Figure 2: Survey area location on Google Earth.

The Bayhorse Idaho/Oregon Geophysics survey area was flown in a north to south (N-000° / N-180° E azimuth) direction with traverse line spacing of 100 metres as depicted in Figure 3. Tie lines were flown perpendicular to the traverse lines at 1000 metre spacing.

For more detailed information on the flight spacings and line directions, see Table 1.

## 1.3 TOPOGRAPHIC RELIEF AND CULTURAL FEATURES

Topographically, the Bayhorse Idaho/Oregon Geophysics survey area exhibits rugged relief with elevations ranging from 612 to 1163 metres above mean sea level over an area of 7 square kilometres (Figure 3).

There are lakes and rivers in and around the survey area, along with signs of culture such as roads.

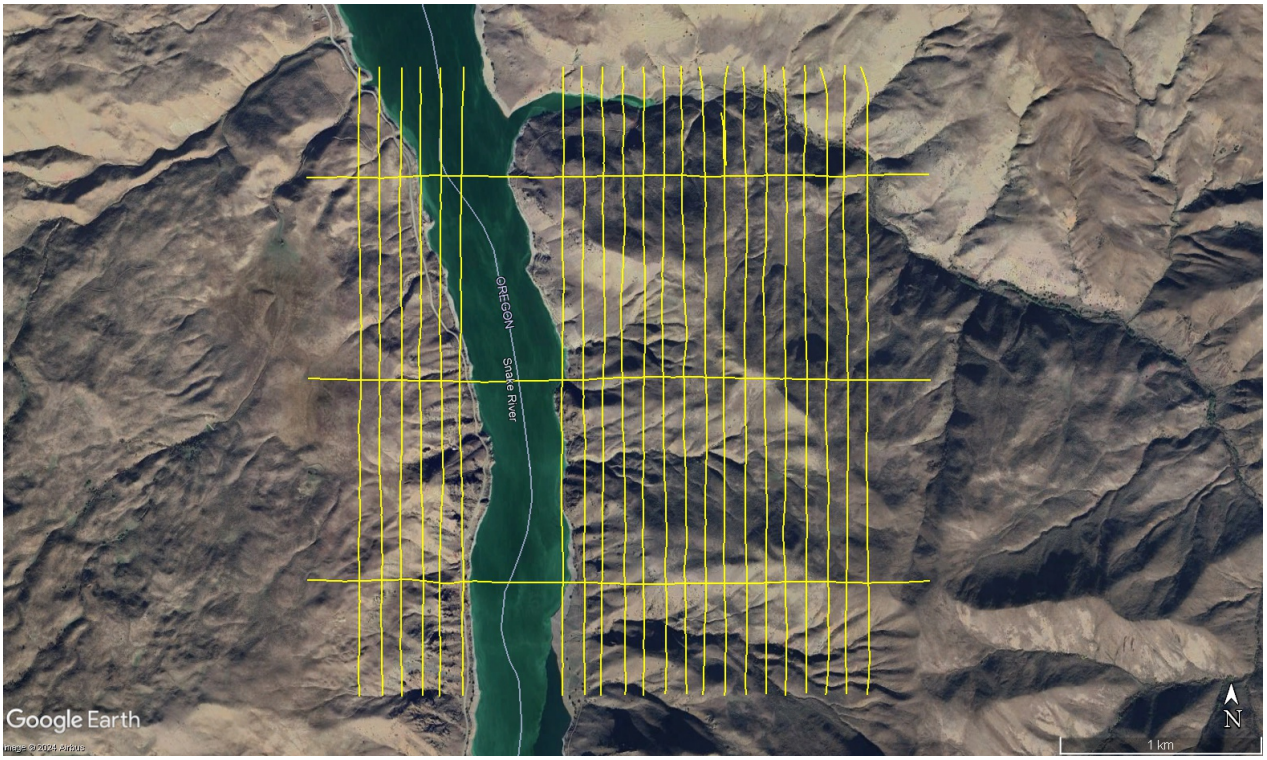



Figure 3: Flight path over a Google Earth Image.

# 2. DATA ACQUISITION

## 2.1 SURVEY AREA

The survey area (see Figure 3 and Appendix A) and general flight specifications are as follows:

Table 1: Survey Specifications

| Survey block | Line spacing (m) | Area ($Km^2$) | Planned [1] Line-km | Actual Line-km | Flight direction | Line numbers |
|---|---|---|---|---|---|---|
| Bayhorse Idaho/Oregon Geophysics Project | Traverse: 100 | 7 | 75 | 78 | N 000° E / N 180° E | L1000 – L1210 |
| | Tie: 1000 | | | | N 090° E / N 270° E | T2000 – T2020 |

Survey area boundaries co-ordinates are provided in Appendix B.

## 2.2 SURVEY OPERATIONS

Survey operations were based out of Baker City, Oregon from January 5th until January 17th, 2024. The following table shows the timing of the flying.

Table 2: Survey Schedule

| Date | Comments |
|---|---|
| 05 Jan 2024 | Crew, equipment, and helicopter arrived onsite in Baker City, OR. Base stations set up and sampled. Recon flight completed. |
| 06 Jan 2024 | No production flights possible due to snow, low ceilings all day. Local logistics. |
| 07 Jan 2024 | No production flights possible due to snow, low ceilings all day. |
| 08 Jan 2024 | No production flights possible due to snow, low ceilings all day. |
| 09 Jan 2024 | No production flights possible due to snow, low ceilings all day. |
| 10 Jan 2024 | No production flights possible due to snow, low ceilings all day. |
| 11 Jan 2024 | No production flights possible due to snow, low ceilings all day. |
| 12 Jan 2024 | No production flights possible due to snow, low ceilings all day. |
| 13 Jan 2024 | No production flights possible due to snow, low ceilings all day. |
| 14 Jan 2024 | No production flights possible due to snow, low ceilings all day. |
| 15 Jan 2024 | Production flight; 72 km flown. One production flight completed. One 3km line not recorded properly in navigation system. |
| 16 Jan 2024 | Production flight; 3 km flown. One production flight completed. Flight path completed. |
| 17 Jan 2024 | Demobilization. |

## 2.3 FLIGHT SPECIFICATIONS

During the survey, the helicopter was maintained at a mean altitude of 91 metres above the ground with an average survey speed of 73 km/hour. This allowed for an average Transmitter-receiver loop terrain clearance of 55 metres and a magnetic sensor clearance of 65 metres.

[1] Note: Actual Line kilometres represent the total line kilometres in the final database. These line-km normally exceed the Planned Line-km, as indicated in the survey NAV files.

The on-board operator was responsible for monitoring the system integrity. He also maintained a detailed flight log during the survey, tracking the times of the flight as well as any unusual geophysical or topographic features.

On return of the aircrew to the base camp the survey data was transferred from a compact flash card (PCMCIA) to the data processing computer. The data were then uploaded via ftp to the Geotech office in Aurora for daily quality assurance and quality control by qualified personnel.

## 2.4 AIRCRAFT AND EQUIPMENT

### 2.4.1 SURVEY AIRCRAFT

The survey was flown using Eurocopter Aerospatiale (A Star) 350 B3 helicopter, registration C-GTEQ. The helicopter is owned and operated by Geotech Aviation Ltd. Installation of the geophysical and ancillary equipment was carried out by a Geotech Ltd crew.

### 2.4.2 ELECTROMAGNETIC SYSTEM

The electromagnetic system was a Geotech Time Domain EM (VTEM™ Plus) full receiver-waveform streamed data recorded system. The "full waveform VTEM system" uses the streamed half-cycle recording of transmitter and receiver waveforms to obtain a complete system response calibration throughout the entire survey flight. VTEM system with the serial number 18 was used for the survey. The VTEM™ transmitter current waveform is shown diagrammatically in Figure 4.

The VTEM™ Receiver and transmitter coils were in concentric-coplanar and Z-direction oriented configuration. The receiver system for the project also included coincident-coaxial X & Y-direction coils to measure the in-line and cross-line dB/dt and calculate B-Field responses. The Transmitter-receiver loop was towed at a mean distance of 36 metres below the aircraft as shown in Figure 5.

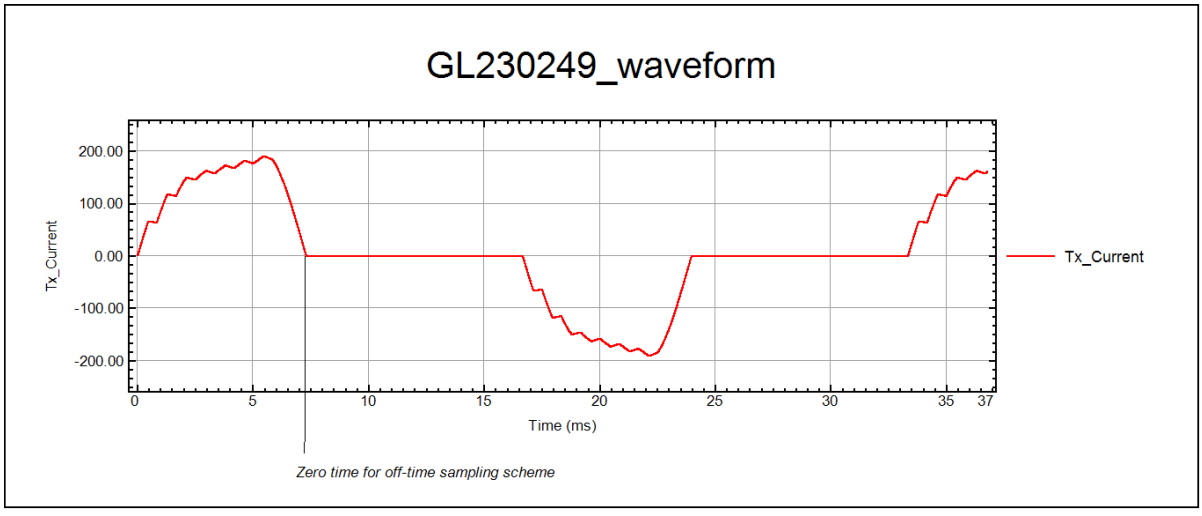



Figure 4: VTEM™ Transmitter Current Waveform

The VTEM™ decay sampling scheme is shown in Table 3 below. Forty-three time measurement gates were used for the final data processing in the range from 0.021 to 8.083 msec. Zero time for the off-time sampling scheme is equal to the current pulse width and is defined as the time near the end of the turn-off ramp where the dI/dt waveform falls to 1/2 of its peak value.

Table 3: Off-Time Decay Sampling Scheme

| VTEM™ Decay Sampling Scheme | | | | |
|---|---|---|---|---|
| Index | Start | End | Middle | Width |
| | Milliseconds | | | |
| 4 | 0.018 | 0.023 | 0.021 | 0.005 |
| 5 | 0.023 | 0.029 | 0.026 | 0.005 |
| 6 | 0.029 | 0.034 | 0.031 | 0.005 |
| 7 | 0.034 | 0.039 | 0.036 | 0.005 |
| 8 | 0.039 | 0.045 | 0.042 | 0.006 |
| 9 | 0.045 | 0.051 | 0.048 | 0.007 |
| 10 | 0.051 | 0.059 | 0.055 | 0.008 |
| 11 | 0.059 | 0.068 | 0.063 | 0.009 |
| 12 | 0.068 | 0.078 | 0.073 | 0.010 |
| 13 | 0.078 | 0.090 | 0.083 | 0.012 |
| 14 | 0.090 | 0.103 | 0.096 | 0.013 |
| 15 | 0.103 | 0.118 | 0.110 | 0.015 |
| 16 | 0.118 | 0.136 | 0.126 | 0.018 |
| 17 | 0.136 | 0.156 | 0.145 | 0.020 |
| 18 | 0.156 | 0.179 | 0.167 | 0.023 |
| 19 | 0.179 | 0.206 | 0.192 | 0.027 |
| 20 | 0.206 | 0.236 | 0.220 | 0.030 |
| 21 | 0.236 | 0.271 | 0.253 | 0.035 |
| 22 | 0.271 | 0.312 | 0.290 | 0.040 |
| 23 | 0.312 | 0.358 | 0.333 | 0.046 |
| 24 | 0.358 | 0.411 | 0.383 | 0.053 |
| 25 | 0.411 | 0.472 | 0.440 | 0.061 |
| 26 | 0.472 | 0.543 | 0.505 | 0.070 |
| 27 | 0.543 | 0.623 | 0.580 | 0.081 |
| 28 | 0.623 | 0.716 | 0.667 | 0.093 |
| 29 | 0.716 | 0.823 | 0.766 | 0.107 |
| 30 | 0.823 | 0.945 | 0.880 | 0.122 |
| 31 | 0.945 | 1.086 | 1.010 | 0.141 |
| 32 | 1.086 | 1.247 | 1.161 | 0.161 |
| 33 | 1.247 | 1.432 | 1.333 | 0.185 |
| 34 | 1.432 | 1.646 | 1.531 | 0.214 |
| 35 | 1.646 | 1.891 | 1.760 | 0.245 |
| 36 | 1.891 | 2.172 | 2.021 | 0.281 |
| 37 | 2.172 | 2.495 | 2.323 | 0.323 |

| VTEM™ Decay Sampling Scheme | | | | |
|---|---|---|---|---|
| Index | Start | End | Middle | Width |
| Milliseconds | | | | |
| 38 | 2.495 | 2.865 | 2.667 | 0.370 |
| 39 | 2.865 | 3.292 | 3.063 | 0.427 |
| 40 | 3.292 | 3.781 | 3.521 | 0.490 |
| 41 | 3.781 | 4.341 | 4.042 | 0.560 |
| 42 | 4.341 | 4.987 | 4.641 | 0.646 |
| 43 | 4.987 | 5.729 | 5.333 | 0.742 |
| 44 | 5.729 | 6.581 | 6.125 | 0.852 |
| 45 | 6.581 | 7.560 | 7.036 | 0.979 |
| 46 | 7.560 | 8.685 | 8.083 | 1.125 |

Z Component: 4 - 46 time gates
X & Y Components: 20 - 46 time gates

Table 4: VTEM™ System Specifications

| Transmitter | Receiver |
|---|---|
| • Transmitter loop diameter: 26 m<br>• Number of turns: 4<br>• Effective Transmitter loop area: 2140.08 $m^2$<br>• Transmitter base frequency: 30 Hz<br>• Peak current: 190 A<br>• Pulse width: 7.3 ms<br>• Waveform shape: Bi-polar trapezoid<br>• Peak dipole moment: 406615.68 nIA<br>• Average transmitter-receiver loop terrain clearance: 55 metres | • X-Coil diameter: 0.32 m<br>• Number of turns: 245<br>• Effective coil area: 19.69 $m^2$<br><br>• Y-Coil diameter: 0.32 m<br>• Number of turns: 245<br>• Effective coil area: 19.69 $m^2$<br><br>• Z-Coil diameter: 1.2 m<br>• Number of turns: 100<br>• Effective coil area: 113.04 $m^2$ |

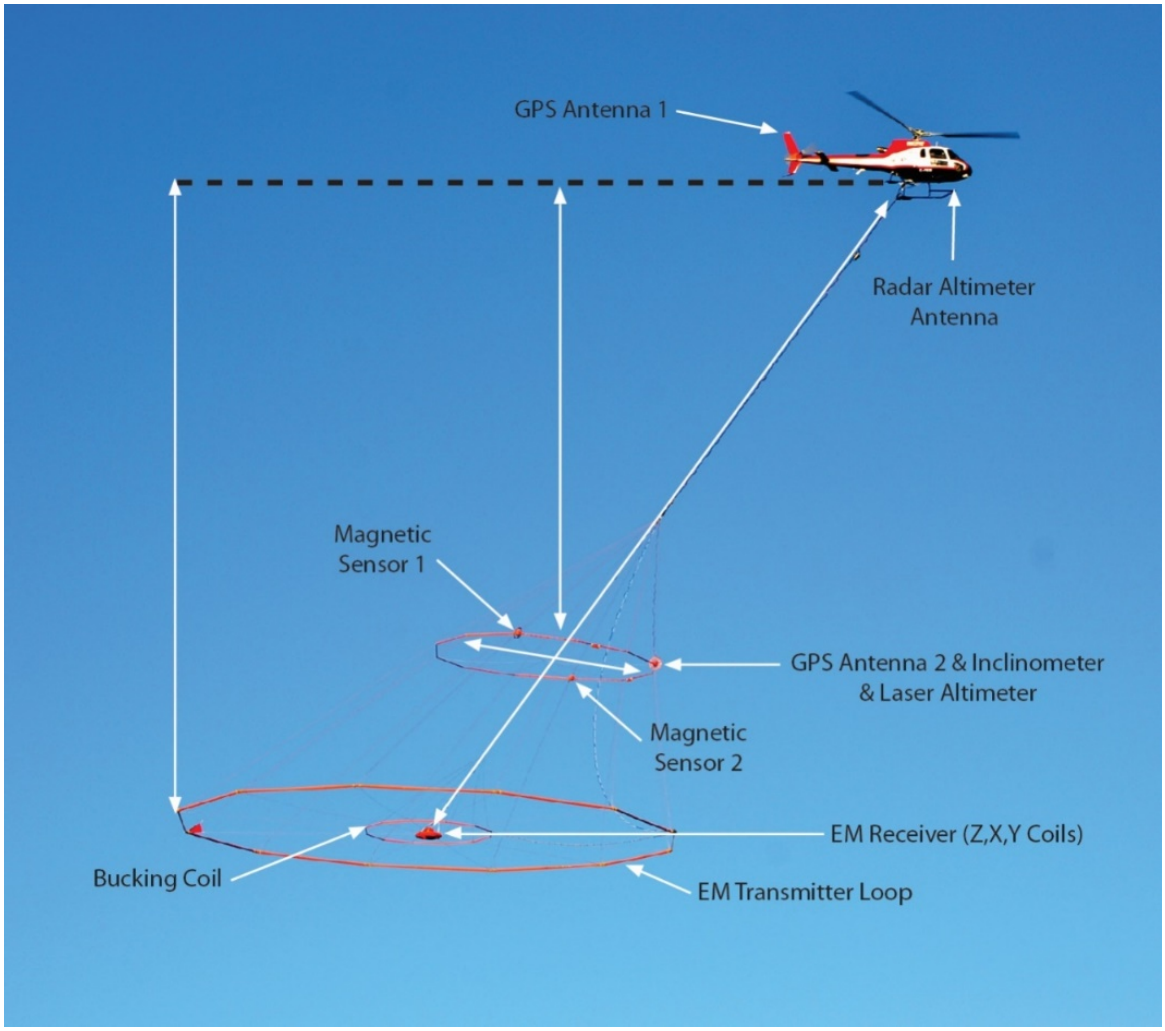



Figure 5: VTEM™plus System Configuration.

### 2.4.3 Full Waveform VTEM™ Sensor Calibration

The calibration is performed on the complete VTEM™ system installed in and connected to the helicopter, using special calibration equipment. This calibration takes place on the ground at the start of the project prior to surveying.

The procedure takes half-cycle files acquired and calculates a calibration file consisting of a single stacked half-cycle waveform. The purpose of the stacking is to attenuate natural and man-made magnetic signals, leaving only the response to the calibration signal.

This calibration allows the transfer function between the EM receiver and data acquisition system and also the transfer function of the current monitor and data acquisition system to be determined. These calibration results are then used in VTEM full waveform processing.

### 2.4.4 Horizontal Magnetic Gradiometer

The horizontal magnetic gradiometer consists of two Geometrics split-beam field magnetic sensors with a sampling interval of 0.1 seconds. These sensors are mounted 12.5 metres apart on a separate loop, 10 metres above the Transmitter-receiver loop. A GPS antenna and Gyro Inclinometer is installed on the separate loop to accurately record the tilt and position of the magnetic gradiometer sensors.

### 2.4.5 Radar Altimeter

A Terra TRA 3000/TRI 40 radar altimeter was used to record terrain clearance. The antenna was mounted beneath the bubble of the helicopter cockpit (Figure 5).

### 2.4.6 GPS Navigation System

The navigation system used was a Geotech PC104 based navigation system utilizing a NovAtel WAAS (Wide Area Augmentation System) enabled GPS receiver, Geotech navigate software, a full screen display with controls in front of the pilot to direct the flight and a NovAtel GPS antenna mounted on the helicopter tail (Figure 5). As many as 11 GPS and two WAAS satellites may be monitored at any one time. The positional accuracy or circular error probability (CEP) is 1.8 m, with WAAS active, it is 1.0 m. The co-ordinates of the survey area were set up prior to the survey and the information was fed into the airborne navigation system. The second GPS antenna is installed on the additional magnetic loop together with Gyro Inclinometer.

### 2.4.7 DIGITAL ACQUISITION SYSTEM

A Geotech data acquisition system recorded the digital survey data on an internal compact flash card. Data is displayed on an LCD screen as traces to allow the operator to monitor the integrity of the system. The data type and sampling interval as provided in Table 5.

Table 5: Acquisition Sampling Rates

| Data Type | Sampling |
|---|---|
| TDEM | 0.1 sec |
| Magnetometer | 0.1 sec |
| GPS Position | 0.2 sec |
| Radar Altimeter | 0.2 sec |
| Inclinometer | 0.1 sec |

## 2.5 BASE STATION

A combined magnetometer/GPS base station was utilized on this project. A Geometrics Caesium vapour magnetometer was used as a magnetic sensor with a sensitivity of 0.001 nT. The base station was recording the magnetic field together with the GPS time at 1 Hz on a base station computer.

The base station magnetometer sensor was installed at a secured location near the landing zone at 044° 50.0546' N, 117° 48.4123' W; away from electric transmission lines and moving ferrous objects such as motor vehicles. The base station data were backed-up to the data processing computer at the end of each survey day.

# 3. PERSONNEL

The following Geotech Ltd. personnel were involved in the project.

FIELD:

| | |
|---|---|
| Project Manager: | Tristan Rice (Office) |
| Data QC: | Nick Venter |
| Crew chief: | Viktor Shevchenko |
| Operator: | Daniel Canas |

The survey pilot and the mechanical engineer were employed directly by Geotech Aviation.

| | |
|---|---|
| Pilot: | Andre Vandrie |
| Mechanical Engineer: | N/A |

OFFICE:

| | |
|---|---|
| Preliminary Data Processing: | Nick Venter |
| Final Data Processing: | Moslem Azarpour |
| Data QA/QC: | TaiChyi Shei |
| Reporting/Mapping: | Ruya Emen |
| Final Review: | Gaurav Nailwal<br>Jean Legault |

Processing phases were carried out under the supervision of Jean M. Legault, Chief Geophysicist. The customer relations were looked after by David Hitz.

# 4. DATA PROCESSING AND PRESENTATION

Data compilation and processing were carried out by the application of Geosoft OASIS Montaj and programs proprietary to Geotech Ltd.

## 4.1 FLIGHT PATH

The flight path, recorded by the acquisition program as WGS 84 latitude/longitude, was converted into the WGS 84 Datum, UTM Zone 11 North coordinate system in Oasis Montaj.

The flight path was drawn using linear interpolation between x, y positions from the navigation system. Positions are updated every second and expressed as UTM easting's (x) and UTM northing's (y).

## 4.2 ELECTROMAGNETIC DATA

The Full Waveform EM specific data processing operations included:

- Half cycle stacking (performed at time of acquisition);
- System response correction;
- Parasitic and drift removal.

A three stage digital filtering process was used to reject major sferic events and to reduce noise levels. Local sferic activity can produce sharp, large amplitude events that cannot be removed by conventional filtering procedures. Smoothing or stacking will reduce their amplitude but leave a broader residual response that can be confused with geological phenomena. To avoid this possibility, a computer algorithm searches out and rejects the major sferic events.

The signal to noise ratio was further improved by the application of a low pass linear digital filter. This filter has zero phase shift which prevents any lag or peak displacement from occurring, and it suppresses only variations with a wavelength less than about 1 second or 15 metres. This filter is a symmetrical 1 sec linear filter.

The results are presented as stacked profiles of EM voltages for the time gates, in linear - logarithmic scale for the B-field and dB/dt responses in the Z component. B-field Z component time channel 25 recorded at 0.440 milliseconds after the termination of the impulse is also presented as a colour image. Calculated Time Constant (TAU) with Calculated Magnetic Vertical Derivative contours is presented in Appendix C and E. Resistivity Depth Image (RDI) is also presented in Appendix F and G.

VTEM™ has three receiver coil orientations. Z-axis coil is oriented parallel to the transmitter coil axis, and both are horizontal to the ground. The X-axis coil is oriented parallel to the ground and along the line-of-flight. The Y-axis coil is oriented parallel to the ground and across the line-of-flight. The combination of the three coils configuration provides information on the position, depth, dip and thickness of a conductor. Generalized modeling results of VTEM data, are shown in Appendix D.

In general X-component data produce cross-over type anomalies: from "+ to – "in flight direction of flight for "thin" sub vertical targets and from "- to +" in direction of flight for "thick" targets. Z component data produce double peak type anomalies for "thin" sub vertical targets and single peak for "thick" targets.

Because the X component polarity is dependent on the flight line direction, a convolution Fraser Filter (Figure 6) is applied to X component data. In this case positive FF anomalies always correspond to "plus-to-minus" X data crossovers independent of the flight line direction.

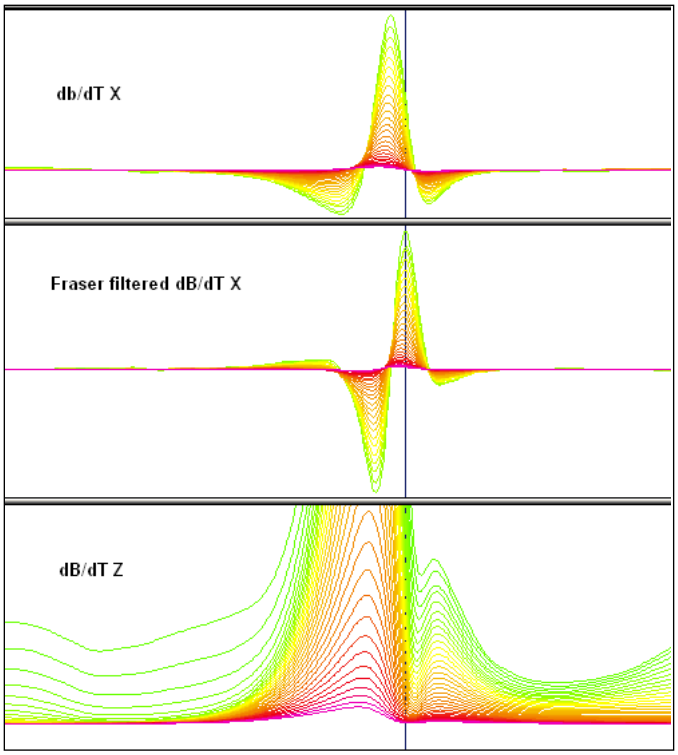



Figure 6: X, Fraser filtered X and Z components for a "thin" sub-vertical conductor.

## 4.3 HORIZONTAL MAGNETIC GRADIOMETER DATA

The horizontal gradients data from the VTEM™ Plus are measured by two magnetometers 12.5 m apart on an independent bird mounted 10m above the VTEM™ loop. A GPS and a Gyro Inclinometer help to determine the positions and orientations of the magnetometers. The data from the two magnetometers are corrected for position and orientation variations, as well as for the diurnal variations using the base station data.

The position of the centre of the horizontal magnetic gradiometer bird is calculated from the GPS utilizing in-house processing tool in Geosoft. Following that total magnetic intensity is calculated at the center of the bird by calculating the mean values from both sensors. In addition to the total intensity advanced processing is done to calculate the in-line and crossline (or lateral) horizontal gradient which enhance the understanding of magnetic targets. The in-line (longitudinal) horizontal gradient is calculated from the difference of two consecutive total magnetic field readings divided by the distance along the flight line direction, while the crossline (lateral) horizontal magnetic gradient is calculated from the difference in the magnetic readings from both magnetic sensors divided by their horizontal separation.

Two advanced magnetic derivative products, the total horizontal derivative (THDR), and tilt angle derivative are also created. The total horizontal derivative or gradient is defined as:

THDR = sqrt (Hx*Hx+Hy*Hy), where Hx and Hy are crossline and in-line horizontal gradients.

The tilt angle derivative (TDR) is defined as:

TDR = arctan (Vz/THDR), where THDR is the total horizontal derivative, and Vz is the vertical derivative.

Measured crossline gradients can help to enhance crossline linear features during gridding.

The processing of the magnetic data involved the correction for diurnal variations by using the digitally recorded ground base station magnetic values. The base station magnetometer data was edited and merged into the Geosoft GDB database on a daily basis. The aeromagnetic data was corrected for diurnal variations by subtracting the observed magnetic base station deviations.

Tie line levelling was carried out by adjusting intersection points along traverse lines. A micro-levelling procedure was applied to remove persistent low-amplitude components of flight-line noise remaining in the data.

The corrected magnetic data was interpolated between survey lines using a random point gridding method to yield x-y grid values for a standard grid cell size of 25 metres at the mapping scale. The Minimum Curvature algorithm was used to interpolate values onto a rectangular regular spaced grid.

## 4.4 TAU PARAMETER AND CVG

The processed VTEM survey results are presented as a calculated dB/dt Z-Component time constant (Tau), which is an indicator of geological unit's electrical conductance.

An explanation of the EM time constant calculation is provided in Appendix E. The TAU dB/dt map is presented in Appendix C. The map is accompanied by an overlay of the calculated vertical gradient of TMI anomaly contours for tracing possible EM-MAG anomaly correlations.

The CVG contour layer, on the top of TAU color grid, is generally more representative of the smaller scale and shallower magnetic sources in comparison with the TMI. The calculated vertical derivative (CVG) is designed to emphasize structures and lithological units that may not otherwise be seen on the TMI due to the nearby presence of stronger magnetic responses, showing a high resolution in terms of individual structures.

# 5. DELIVERABLES

## 5.1 SURVEY REPORT

The survey report describes the data acquisition, processing, and final presentation of the survey results. The survey report is provided in two paper copies and digitally in PDF format.

## 5.2 MAPS

Maps were produced at scale of 1:5,000 for best representation of the survey size and line spacing. The coordinate/projection system used was WGS84 Datum, UTM Zone 11N. All maps show the flight path trace and topographic data; latitude and longitude are also noted on maps.

The results of the survey are presented as EM profiles, a late-time gate gridded EM channel, and a colour magnetic TMI contour map.

- Maps at 1:5,000 in Geosoft MAP format, as follows:

| | |
|---|---|
| GL230249_**_dBdt: | dB/dt profiles Z Component, Time Gates 0.220 – 7.036 ms in linear – logarithmic scale. |
| GL230249_**_BField: | B-field profiles Z Component, Time Gates 0.220 – 7.036 ms in linear – logarithmic scale. |
| GL230249_**_BFz25: | B-field late time Z Component Channel 25, Time Gate 0.440 ms colour image. |
| GL230249_**_SFxFF25: | Fraser Filtered dB/dt X Component Channel 25, Time Gate 0.440 ms colour image. |
| GL230249_**_SFz25: | VTEM dB/dt Z Component Channel 25, Time Gate 0.440 ms. |
| GL230249_**_TauSF_CVG: | dB/dtz Calculated Time Constant (Tau) with Calculated Magnetic Vertical Derivative contours. |
| GL230249_**_TMI: | Total magnetic intensity colour image and contours. |
| GL230249_**_CVG: | Calculated Vertical Gradient (CVG) of TMI colour image. |
| GL230249_**_TiltDrv: | Magnetic Tilt Angle Derivative colour image. |
| GL230249_**_TotHG: | Magnetic Total Horizontal Gradient colour image. |
| GL230249_**_PLM: | Power Line Monitor (PLM). |

  Where ** represents client name and map scale.
  E.g., *GL230249_BayhorseSilver_5K_TMI.map*

  Maps are also presented in PDF format.

- The topographic base and inset map data were derived from 1:250,000 CANVEC data. Background shading is from ASTER GDEM (https://gdex.cr.usgs.gov/gdex).

- A Google Earth file *GL230249_BayhorseSilver.kmz* showing the flight path of the blocks is included. Free versions of Google Earth software from: http://earth.google.com/download-earth.html

## 5.3 DIGITAL DATA

Two copies of the data and maps on DVD were prepared to accompany the report. Each DVD contains a digital file of the line data in GDB Geosoft Montaj format as well as the maps in Geosoft Montaj Map and PDF format.

- DVD structure.

  Data contains databases, grids and maps, as described below.
  Report contains a copy of the report and appendices in PDF format.

Databases in Geosoft GDB format, containing the channels listed in Table 6.

Table 6: Geosoft GDB Data Format

| Channel name | Units | Description |
|---|---|---|
| X | metres | UTM Easting WGS84 Zone 11 North |
| Y | metres | UTM Northing WGS84 Zone 11 North |
| Longitude | Decimal Degrees | WGS 84 Longitude data |
| Latitude | Decimal Degrees | WGS 84 Latitude data |
| Z | metres | GPS antenna elevation (above Geoid) |
| Zb | metres | EM bird elevation (above Geoid) |
| Radar | metres | helicopter terrain clearance from radar altimeter |
| Radarb | metres | Calculated EM transmitter-receiver loop terrain clearance from radar altimeter |
| DEM | metres | Digital Elevation Model |
| Gtime | Seconds of the day | GPS time |
| Mag1L | nT | Measured Total Magnetic field data (left sensor) |
| Mag1R | nT | Measured Total Magnetic field data (right sensor) |
| Basemag | nT | Magnetic diurnal variation data |
| Mag2LZ | nT | Z corrected (w.r.t. loop center) and diurnal corrected magnetic field left mag |
| Mag2RZ | nT | Z corrected (w.r.t. loop center) and diurnal corrected magnetic field right mag |
| TMI2 | nT | Diurnal corrected total magnetic field intensity at the centre of the loop |
| TMI3 | nT | Leveled total magnetic field intensity at the centre of the loop |
| CVG | nT/m | Calculated Vertical Derivative Total Magnetic Intensity |
| Hginline | nT/m | Calculated in-line gradient |
| Hgcxline | nT/m | Measured cross-line gradient |
| SFz[4] | pV/(A*m$^4$) | Z dB/dt 0.021 millisecond time channel |
| SFz[5] | pV/(A*m$^4$) | Z dB/dt 0.026 millisecond time channel |
| SFz[6] | pV/(A*m$^4$) | Z dB/dt 0.031 millisecond time channel |
| SFz[7] | pV/(A*m$^4$) | Z dB/dt 0.036 millisecond time channel |
| SFz[8] | pV/(A*m$^4$) | Z dB/dt 0.042 millisecond time channel |
| SFz[9] | pV/(A*m$^4$) | Z dB/dt 0.048 millisecond time channel |
| SFz[10] | pV/(A*m$^4$) | Z dB/dt 0.055 millisecond time channel |
| SFz[11] | pV/(A*m$^4$) | Z dB/dt 0.063 millisecond time channel |
| SFz[12] | pV/(A*m$^4$) | Z dB/dt 0.073 millisecond time channel |

| Channel name | Units | Description |
|---|---|---|
| SFz[13] | pV/(A*m$^4$) | Z dB/dt 0.083 millisecond time channel |
| SFz[14] | pV/(A*m$^4$) | Z dB/dt 0.096 millisecond time channel |
| SFz[15] | pV/(A*m$^4$) | Z dB/dt 0.110 millisecond time channel |
| SFz[16] | pV/(A*m$^4$) | Z dB/dt 0.126 millisecond time channel |
| SFz[17] | pV/(A*m$^4$) | Z dB/dt 0.145 millisecond time channel |
| SFz[18] | pV/(A*m$^4$) | Z dB/dt 0.167 millisecond time channel |
| SFz[19] | pV/(A*m$^4$) | Z dB/dt 0.192 millisecond time channel |
| SFz[20] | pV/(A*m$^4$) | Z dB/dt 0.220 millisecond time channel |
| SFz[21] | pV/(A*m$^4$) | Z dB/dt 0.253 millisecond time channel |
| SFz[22] | pV/(A*m$^4$) | Z dB/dt 0.290 millisecond time channel |
| SFz[23] | pV/(A*m$^4$) | Z dB/dt 0.333 millisecond time channel |
| SFz[24] | pV/(A*m$^4$) | Z dB/dt 0.383 millisecond time channel |
| SFz[25] | pV/(A*m$^4$) | Z dB/dt 0.440 millisecond time channel |
| SFz[26] | pV/(A*m$^4$) | Z dB/dt 0.505 millisecond time channel |
| SFz[27] | pV/(A*m$^4$) | Z dB/dt 0.580 millisecond time channel |
| SFz[28] | pV/(A*m$^4$) | Z dB/dt 0.667 millisecond time channel |
| SFz[29] | pV/(A*m$^4$) | Z dB/dt 0.766 millisecond time channel |
| SFz[30] | pV/(A*m$^4$) | Z dB/dt 0.880 millisecond time channel |
| SFz[31] | pV/(A*m$^4$) | Z dB/dt 1.010 millisecond time channel |
| SFz[32] | pV/(A*m$^4$) | Z dB/dt 1.161 millisecond time channel |
| SFz[33] | pV/(A*m$^4$) | Z dB/dt 1.333 millisecond time channel |
| SFz[34] | pV/(A*m$^4$) | Z dB/dt 1.531 millisecond time channel |
| SFz[35] | pV/(A*m$^4$) | Z dB/dt 1.760 millisecond time channel |
| SFz[36] | pV/(A*m$^4$) | Z dB/dt 2.021 millisecond time channel |
| SFz[37] | pV/(A*m$^4$) | Z dB/dt 2.323 millisecond time channel |
| SFz[38] | pV/(A*m$^4$) | Z dB/dt 2.667 millisecond time channel |
| SFz[39] | pV/(A*m$^4$) | Z dB/dt 3.063 millisecond time channel |
| SFz[40] | pV/(A*m$^4$) | Z dB/dt 3.521 millisecond time channel |
| SFz[41] | pV/(A*m$^4$) | Z dB/dt 4.042 millisecond time channel |
| SFz[42] | pV/(A*m$^4$) | Z dB/dt 4.641 millisecond time channel |
| SFz[43] | pV/(A*m$^4$) | Z dB/dt 5.333 millisecond time channel |
| SFz[44] | pV/(A*m$^4$) | Z dB/dt 6.125 millisecond time channel |
| SFz[45] | pV/(A*m$^4$) | Z dB/dt 7.036 millisecond time channel |
| SFz[46] | pV/(A*m$^4$) | Z dB/dt 8.083 millisecond time channel |
| SFx[20] | pV/(A*m$^4$) | X dB/dt 0.220 millisecond time channel |
| SFx[21] | pV/(A*m$^4$) | X dB/dt 0.253 millisecond time channel |
| SFx[22] | pV/(A*m$^4$) | X dB/dt 0.290 millisecond time channel |
| SFx[23] | pV/(A*m$^4$) | X dB/dt 0.333 millisecond time channel |
| SFx[24] | pV/(A*m$^4$) | X dB/dt 0.383 millisecond time channel |
| SFx[25] | pV/(A*m$^4$) | X dB/dt 0.440 millisecond time channel |
| SFx[26] | pV/(A*m$^4$) | X dB/dt 0.505 millisecond time channel |
| SFx[27] | pV/(A*m$^4$) | X dB/dt 0.580 millisecond time channel |
| SFx[28] | pV/(A*m$^4$) | X dB/dt 0.667 millisecond time channel |
| SFx[29] | pV/(A*m$^4$) | X dB/dt 0.766 millisecond time channel |
| SFx[30] | pV/(A*m$^4$) | X dB/dt 0.880 millisecond time channel |
| SFx[31] | pV/(A*m$^4$) | X dB/dt 1.010 millisecond time channel |
| SFx[32] | pV/(A*m$^4$) | X dB/dt 1.161 millisecond time channel |
| SFx[33] | pV/(A*m$^4$) | X dB/dt 1.333 millisecond time channel |
| SFx[34] | pV/(A*m$^4$) | X dB/dt 1.531 millisecond time channel |

| Channel name | Units | Description |
|---|---|---|
| SFx[35] | pV/(A*m$^4$) | X dB/dt 1.760 millisecond time channel |
| SFx[36] | pV/(A*m$^4$) | X dB/dt 2.021 millisecond time channel |
| SFx[37] | pV/(A*m$^4$) | X dB/dt 2.323 millisecond time channel |
| SFx[38] | pV/(A*m$^4$) | X dB/dt 2.667 millisecond time channel |
| SFx[39] | pV/(A*m$^4$) | X dB/dt 3.063 millisecond time channel |
| SFx[40] | pV/(A*m$^4$) | X dB/dt 3.521 millisecond time channel |
| SFx[41] | pV/(A*m$^4$) | X dB/dt 4.042 millisecond time channel |
| SFx[42] | pV/(A*m$^4$) | X dB/dt 4.641 millisecond time channel |
| SFx[43] | pV/(A*m$^4$) | X dB/dt 5.333 millisecond time channel |
| SFx[44] | pV/(A*m$^4$) | X dB/dt 6.125 millisecond time channel |
| SFx[45] | pV/(A*m$^4$) | X dB/dt 7.036 millisecond time channel |
| SFx[46] | pV/(A*m$^4$) | X dB/dt 8.083 millisecond time channel |
| SFy | pV/(A*m$^4$) | Y dB/dt data for time channels 20 to 46 |
| BFz | (pV*ms)/(A*m$^4$) | Z B-Field data for time channels 4 to 46 |
| BFx | (pV*ms)/(A*m$^4$) | X B-Field data for time channels 20 to 46 |
| BFy | (pV*ms)/(A*m$^4$) | Y B-Field data for time channels 20 to 46 |
| SFxFF | pV/(A*m$^4$) | Fraser Filtered X dB/dt for time channels 20 to 46 |
| NchanBF | | Latest time channels of TAU calculation |
| TauBF | ms | Time constant B-Field |
| NchanSF | | Latest time channels of TAU calculation |
| TauSF | ms | Time constant dB/dt |
| PLM | | 60 Hz power line monitor |

Electromagnetic B-field and dB/dt Z component data is found in array channel format between indexes 4 – 46, and X & Y component data from 20 – 46, as described above.

- Database of the Resistivity Depth Images in Geosoft GDB format, containing the following channels:

Table 7: Geosoft Resistivity Depth Image GDB Data Format

| Channel name | Units | Description |
|---|---|---|
| Xg | metres | UTM Easting WGS84 Zone 11 North |
| Yg | metres | UTM Northing WGS84 Zone 11 North |
| Dist: | metres | Distance from the beginning of the line |
| Depth: | metres | array channel, depth from the surface |
| Z: | metres | array channel, depth from sea level |
| AppRes: | Ohm-m | array channel, Apparent Resistivity |
| TR: | metres | EM system height from sea level |
| Topo: | metres | digital elevation model |
| Radarb: | metres | Calculated EM transmitter-receiver loop terrain clearance from radar altimeter |
| SF: | pV/(A*m^4) | array channel, dBz/dT |
| MAG: | nT | Total Magnetic Intensity data |
| CVG: | nT/m | Calculated Vertical Gradient data |
| DOI: | metres | Depth of Investigation: a measure of VTEM depth effectiveness |
| PLM: | | 60Hz Power Line Monitor |

- Databases of the VTEM Waveforms "GL230249_Waveform.gdb" in Geosoft GDB format, containing the following channels:

Table 8: Geosoft database for the VTEM waveform

| Channel name | Units | Description |
|---|---|---|
| Time: | milliseconds | Sampling rate interval, 5.2083 microseconds |
| Tx_Current: | amps | Output current of the transmitter |

- Geosoft Resistivity Depth Image Products:

| | |
|---|---|
| Sections: | Apparent resistivity sections along each line in .GRD and .PDF format |
| Slices: | Apparent resistivity slices at selected depths from 25m to depth of investigation, at an increment of 25m in .GRD and .PDF format |
| Voxel: | 3D Voxel imaging of apparent resistivity data clipped by digital elevation and depth of investigation |

- Grids in Geosoft GRD and GeoTIFF format, as follows:

| | |
|---|---|
| GL230249_DEM: | Digital Elevation Model (metres) |
| GL230249_PLM | Power Line Monitor (PLM) |
| GL230249_BFz25: | B-Field Z Component Channel 25 (Time Gate 0.440 ms) |
| GL230249_SFxFF25: | Fraser Filtered dB/dt X Component Channel 25 (Time Gate 0.440 ms) |
| GL230249_SFz10: | dB/dt Z Component Channel 10 (Time Gate 0.055 ms) |
| GL230249_SFz25: | dB/dt Z Component Channel 25 (Time Gate 0.440 ms) |
| GL230249_SFz35: | dB/dt Z Component Channel 35 (Time Gate 1.760 ms) |
| GL230249_TauBF: | B-Field Z Component, Calculated Time Constant (ms) |
| GL230249_TauSF: | dB/dt Z Component, Calculated Time Constant (ms) |
| GL230249_TMI3: | Total Magnetic Intensity (nT) |
| GL230249_CVG: | Calculated Vertical Gradient (nT/m) |
| GL230249_Hgcxline | Measured Cross-line Gradient (nT/m) |
| GL230249_Hginline | Measured In-Line Gradient (nT/m) |
| GL230249_TiltDrv: | Magnetic Tilt derivative (radians) |
| GL230249_TotHG: | Magnetic Total Horizontal Gradient (nT/m) |

A Geosoft .GRD file has a .GI metadata file associated with it, containing grid projection information. Grid cell sizes of 25 metres were used.

# 6. CONCLUSIONS AND RECOMMENDATIONS

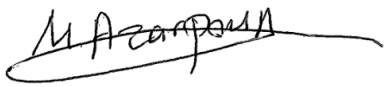
A helicopter-borne versatile time domain electromagnetic (VTEM™ plus) geophysical survey has been completed on behalf of Bayhorse Silver Inc. over the Bayhorse Idaho/Oregon Geophysics Project, situated near Huntington, Oregon & Weiser, Idaho.

The total area coverage is 7 km$^2$ and the total survey line coverage is 78 line-kilometres over one survey block. The principal sensors included a Time Domain EM system, and a horizontal magnetic gradiometer system with two caesium magnetometers. Results have been presented as stacked profiles, and contour colour images at scales of 1:5,000. A formal interpretation has not been included in this report, however, RDI resistivity-depth imaging has been performed in support of the VTEM data.

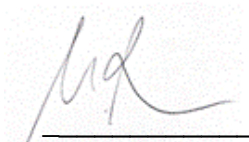
Based on the geophysical results obtained, a number of electromagnetic and magnetic anomalies of interest have been identified over the project area including several mid-late-channel conductive signatures. The relationships between the EM and magnetics are highlighted in our TAU dBz/dt EM decay constant map with magnetic CVG contours (Appendix C) and the RDI resistivity-depth image sections with profiles (Appendix G).

The Bayhorse Idaho/Oregon Geophysics Project is understood to be prospective for silver-gold mineralisation (www.bayhorsesilver.com) and, as a result, both the magnetic and EM data are likely to be of exploration interest. If EM conductors are of interest for the exploration program, we recommend that EM anomaly picking, and Maxwell plate modelling be performed on the anomalies of greatest interest prior to ground follow up and drill testing. For non-conductive targets, more advanced 1D layered earth modelling of the EM data will prove useful in highlighting weakly anomalous resistive and conductive features of interest, as compared to the RDI imaging products being provided. Magnetic CET structural and lineament analysis, as well as 3D MVI magnetic inversions will be useful for mapping structure, alteration, and lithology in 2D-3D space across the blocks. Finally, we recommend that more advanced, integrated interpretation be performed, such as SOM (self-organizing maps) in order to better correlate the 1D EM and 3D Magnetic modelling in 2D-3D and these results further evaluated against the known geology for future targeting.

Respectfully submitted[2],



Moslem Azarpour
**Geotech Ltd.**



Ruya Emen
**Geotech Ltd.**

[2] Final data processing of the EM and magnetic data was carried out by Moslem Azarpour, from the office of Geotech Ltd. in Aurora, Ontario, under the supervision of Jean M. Legault, M.Sc.A, P.Eng, and P.Geo - Chief Geophysicist.

TaiChyi Shei
**Geotech Ltd.**

Gaurav Nailwal
**Geotech Ltd.**




Jean M. Legault, M.Sc.A, P.Eng, P.Geo
**Geotech Ltd.**

February 2024

# APPENDIX A

## SURVEY AREA LOCATION MAP



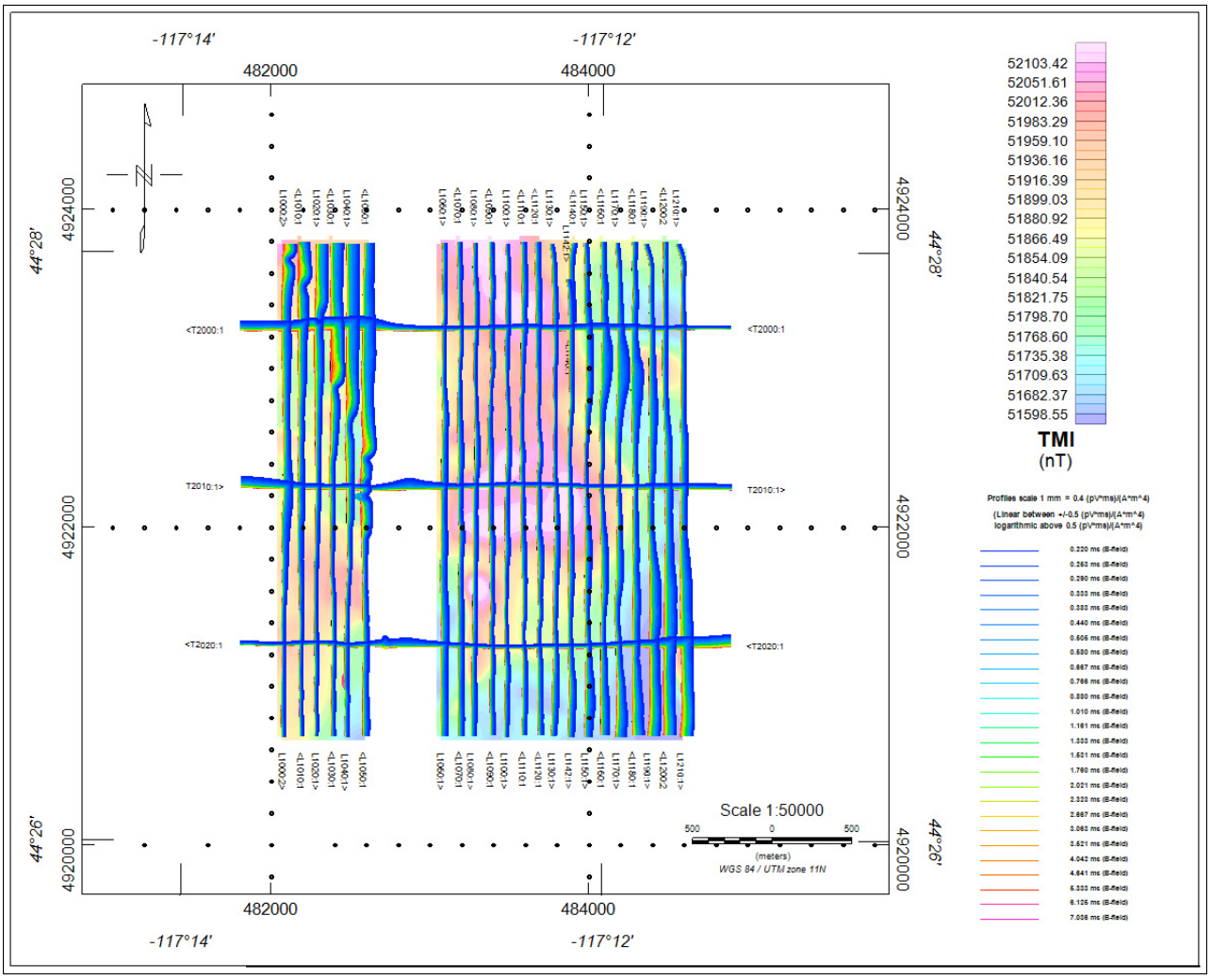

Overview of the Survey Area

# APPENDIX B
## SURVEY AREA COORDINATES
(WGS 84, UTM Zone 11 North)

| X | Y |
|---|---|
| 482045 | 4923788 |
| 482032 | 4923810 |
| 482032 | 4920689 |
| 482617 | 4920685 |
| 482622 | 4923806 |
| 482040 | 4923814 |

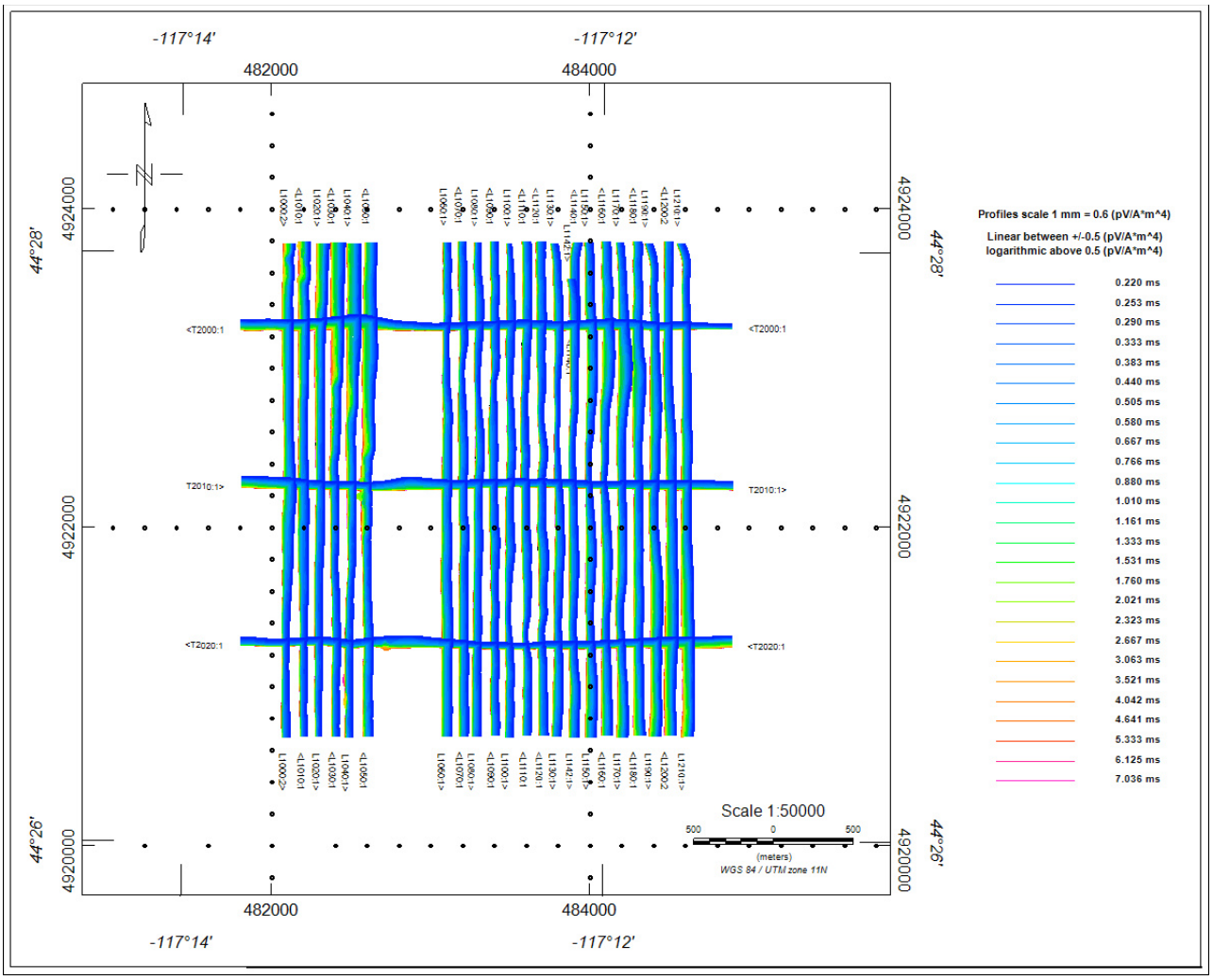
| | |
|---|---|
| 483035 | 4923801 |
| 483035 | 4923801 |
| 483030 | 4920676 |
| 484619 | 4920672 |
| 484611 | 4923806 |
| 483030 | 4923806 |

# APPENDIX C
## GEOPHYSICAL MAPS[1]
## Bayhorse Idaho/Oregon Geophysics Project

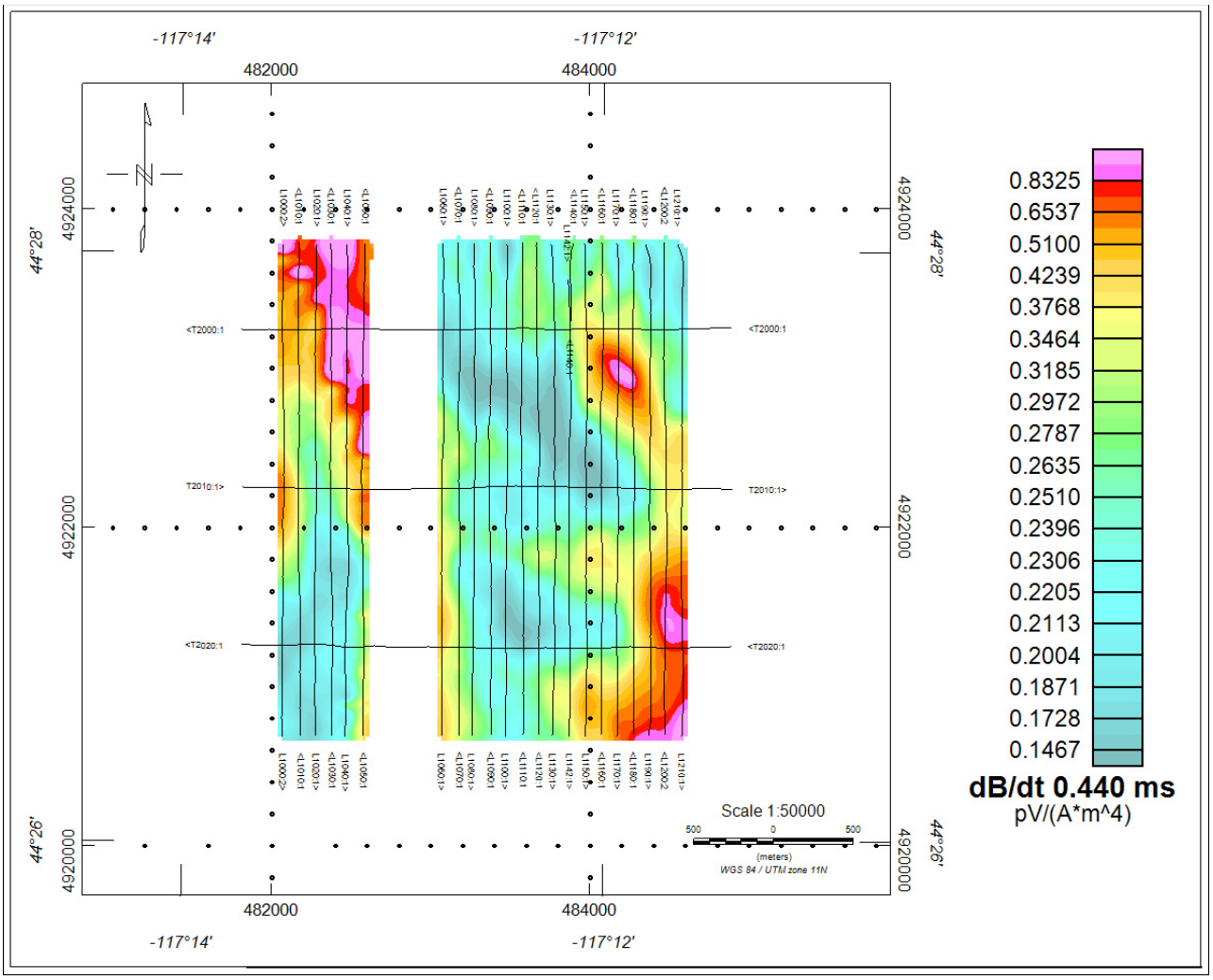



Bayhorse Idaho/Oregon Geophysics Project: B-field profiles Z Component, Time Gates 0.220 – 7.036 ms in linear-logarithmic scale, over Total Magnetic Intensity

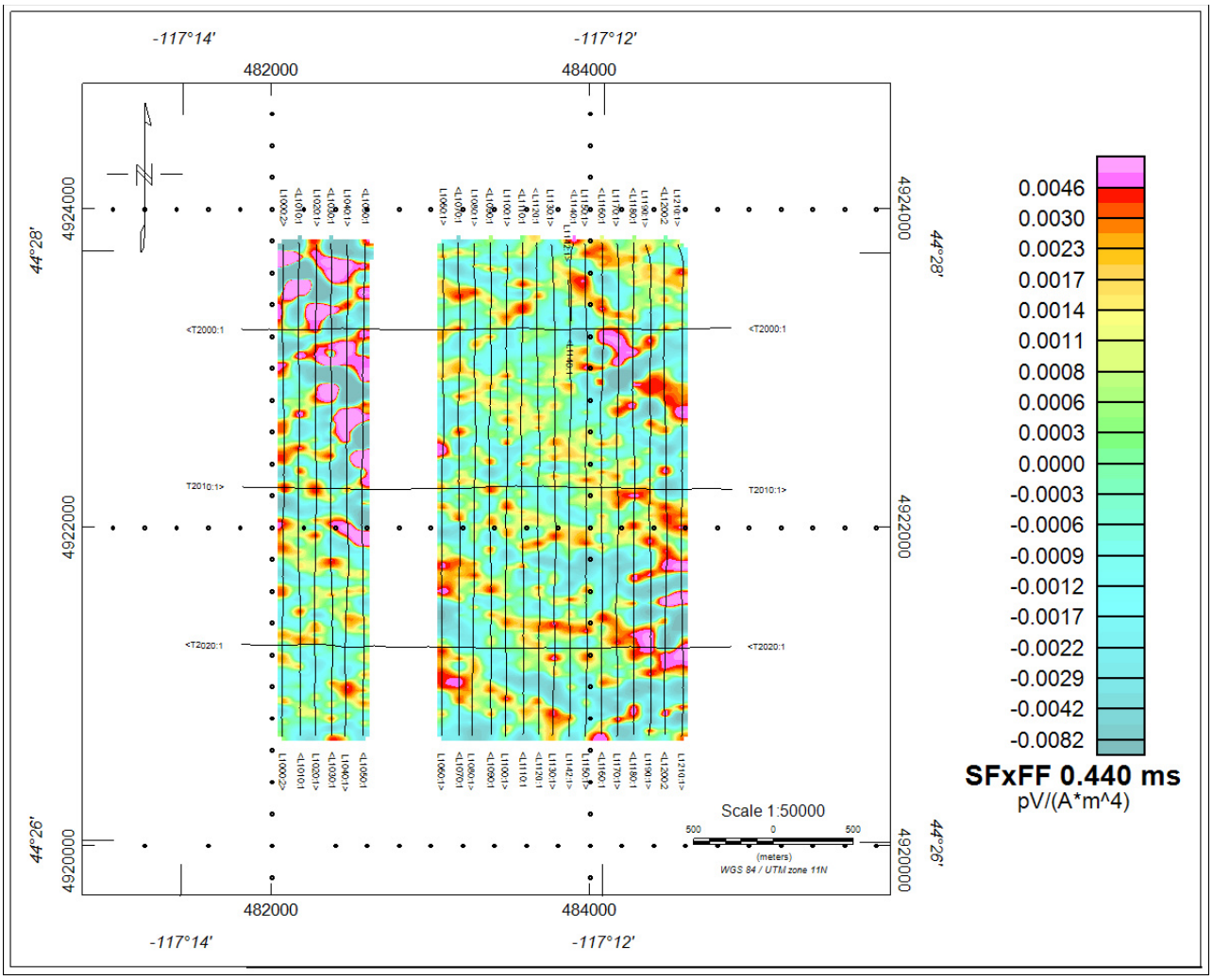
[1] Full size geophysical maps are also available in PDF format on the final DVD



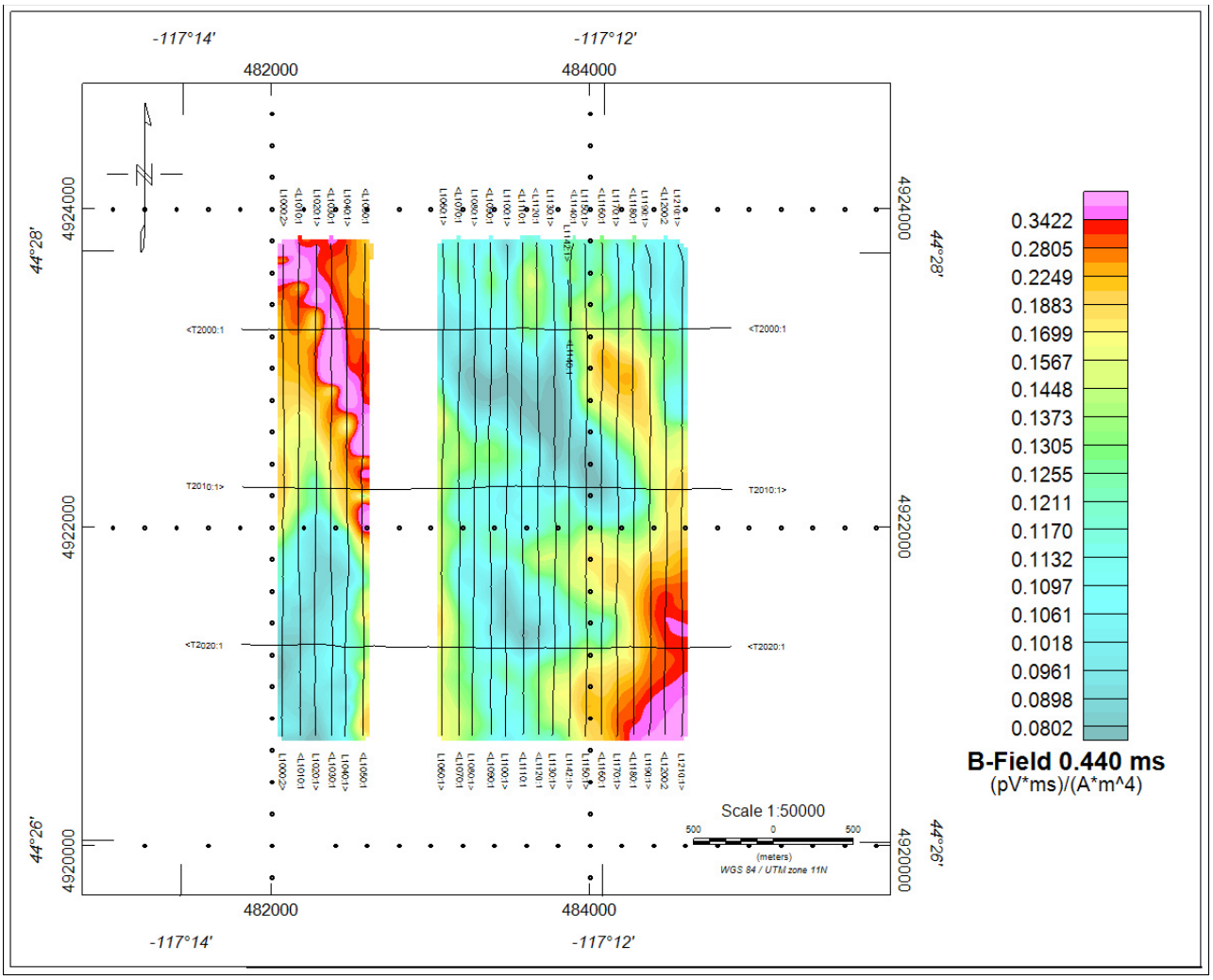

Bayhorse Idaho/Oregon Geophysics Project: dB/dt profiles Z Component, Time Gates 0.220 – 7.036 ms in linear-logarithmic scale



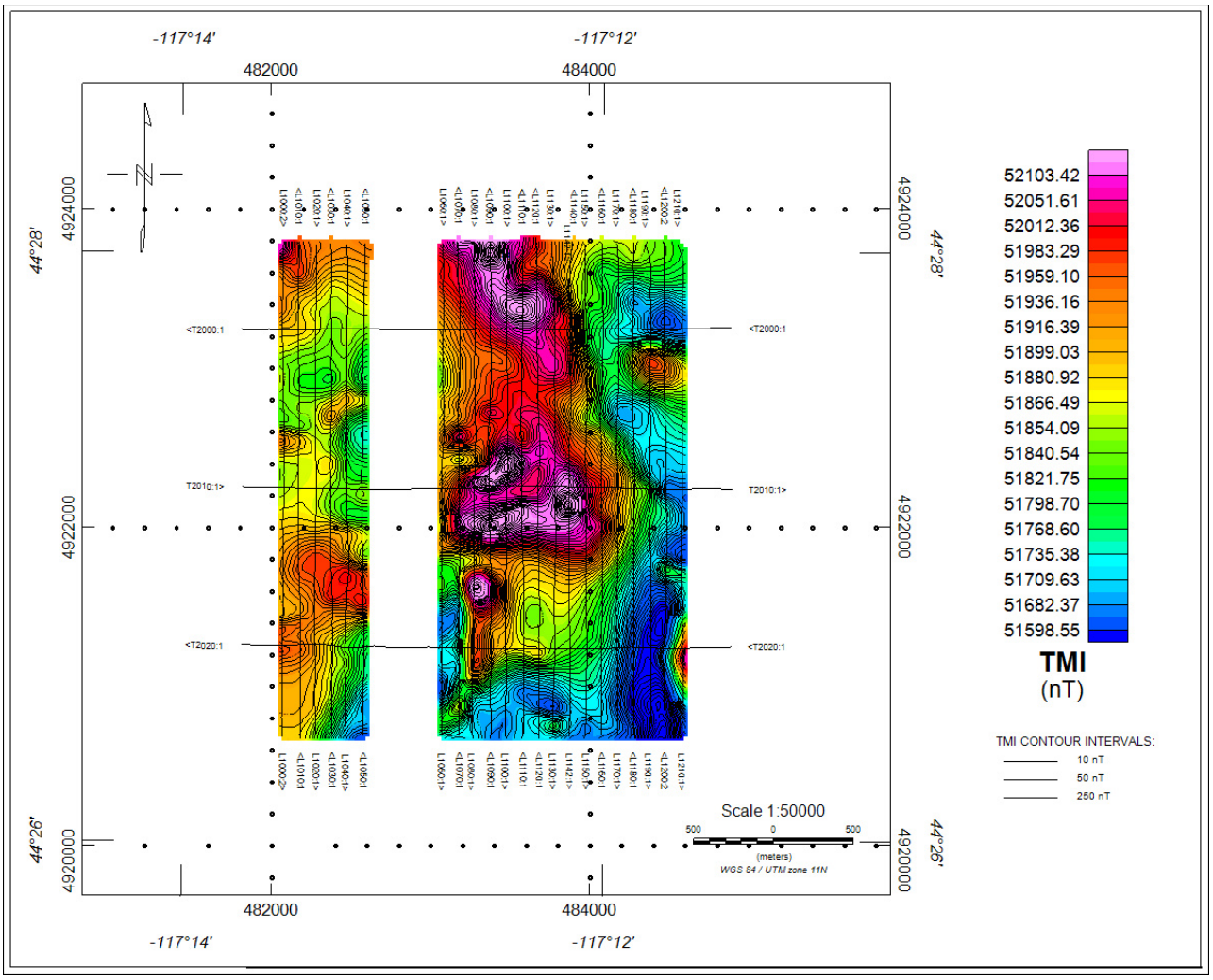

Bayhorse Idaho/Oregon Geophysics Project: dB/dt Z Component Channel 25 (Time Gate 0.440 ms)



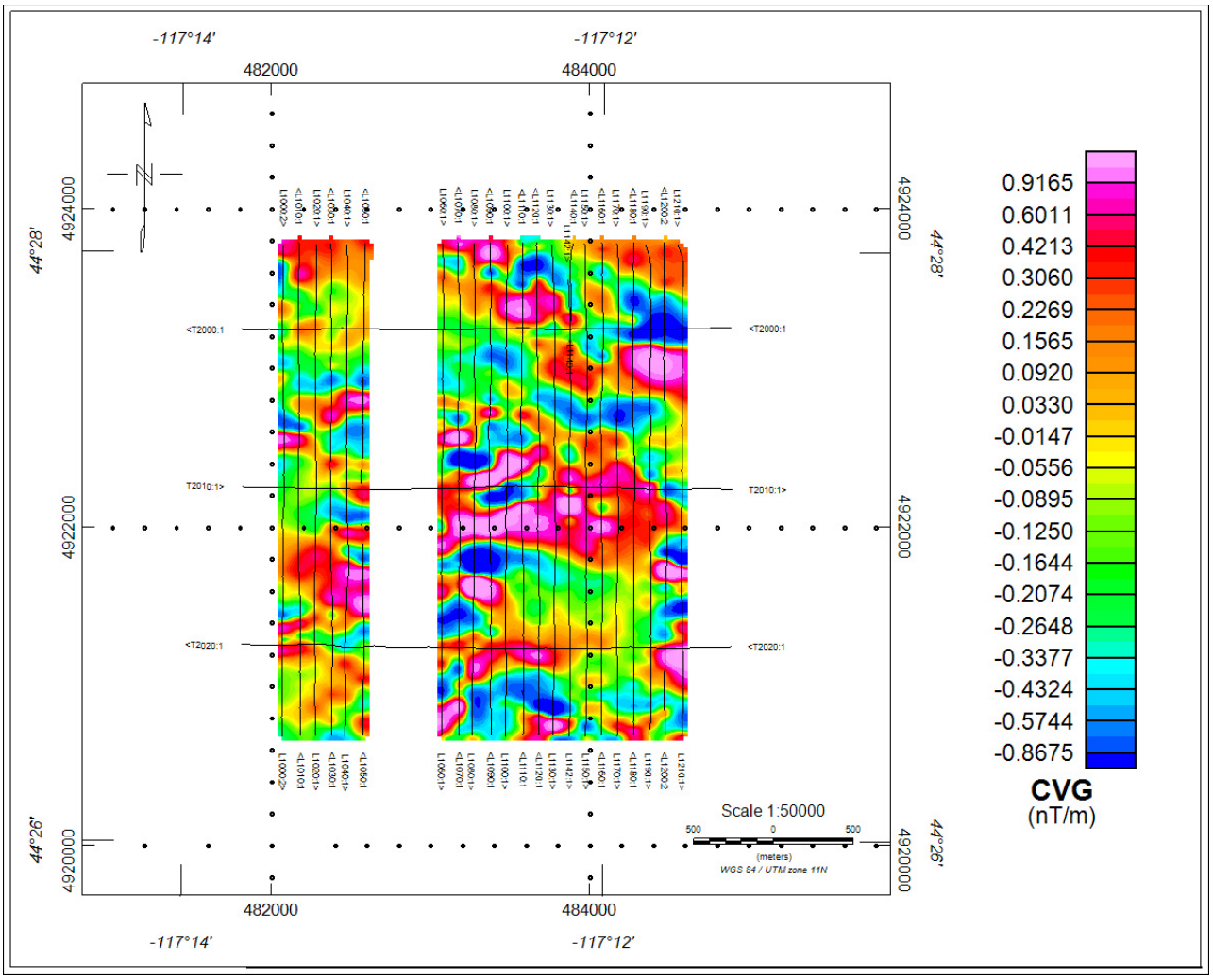

Bayhorse Idaho/Oregon Geophysics Project: Fraser Filtered dB/dt X Component, Channel 25, Time Gate 0.440 ms



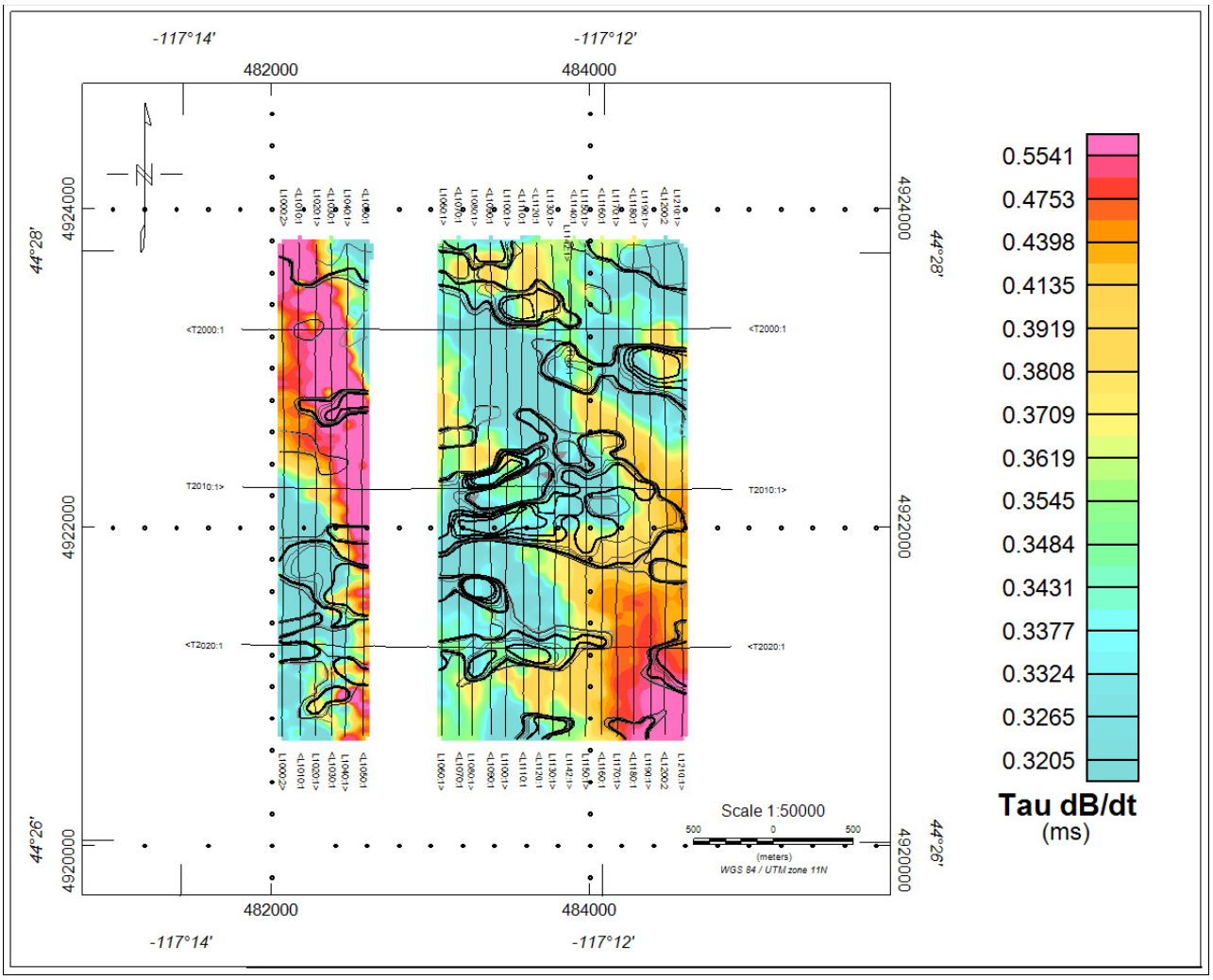

Bayhorse Idaho/Oregon Geophysics Project: VTEM B-Field Z Component Channel 25, Time Gate 0.440 ms



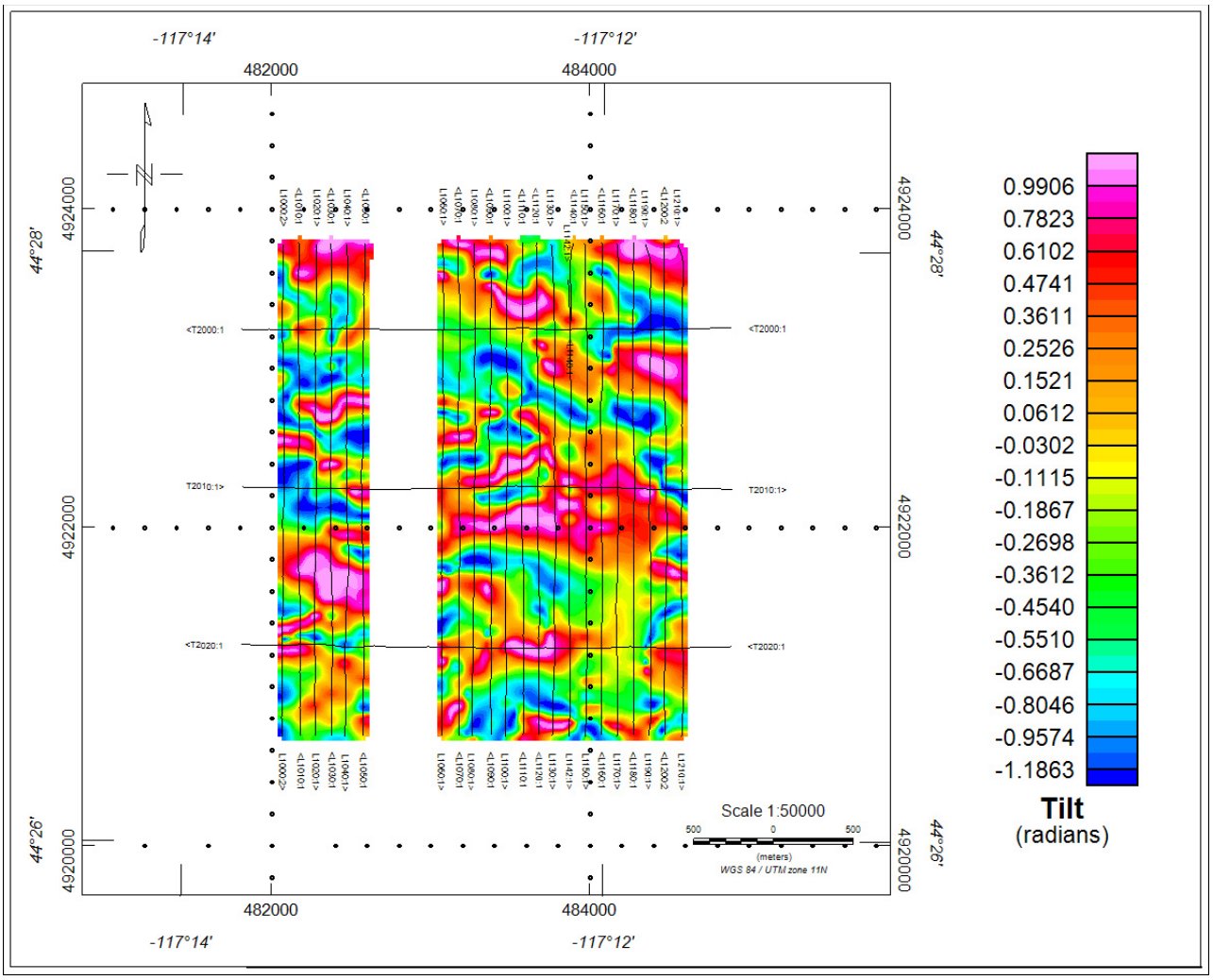

Bayhorse Idaho/Oregon Geophysics Project: Total Magnetic Intensity (TMI)



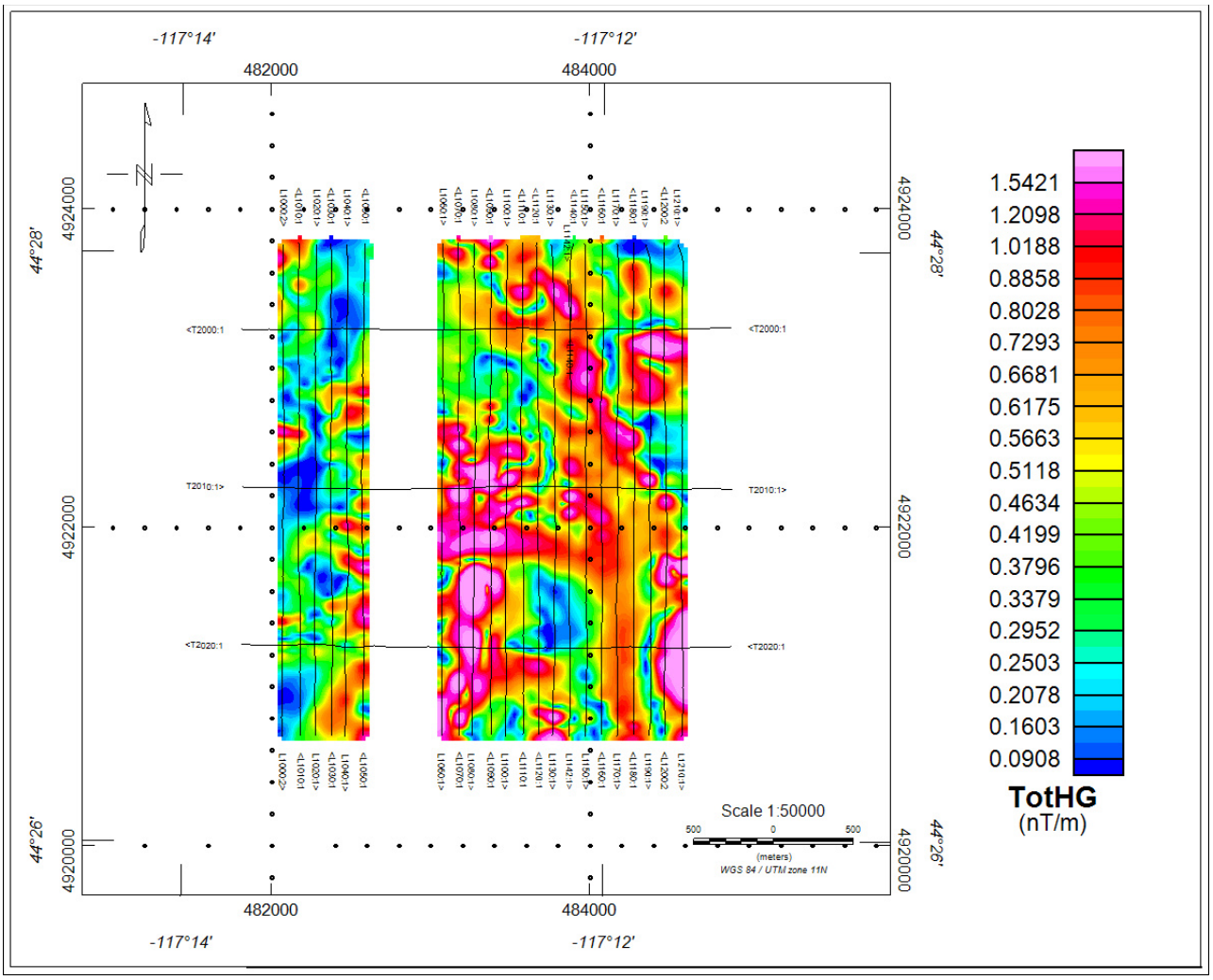

Bayhorse Idaho/Oregon Geophysics Project: Calculated Vertical Magnetic Gradient (CVG)



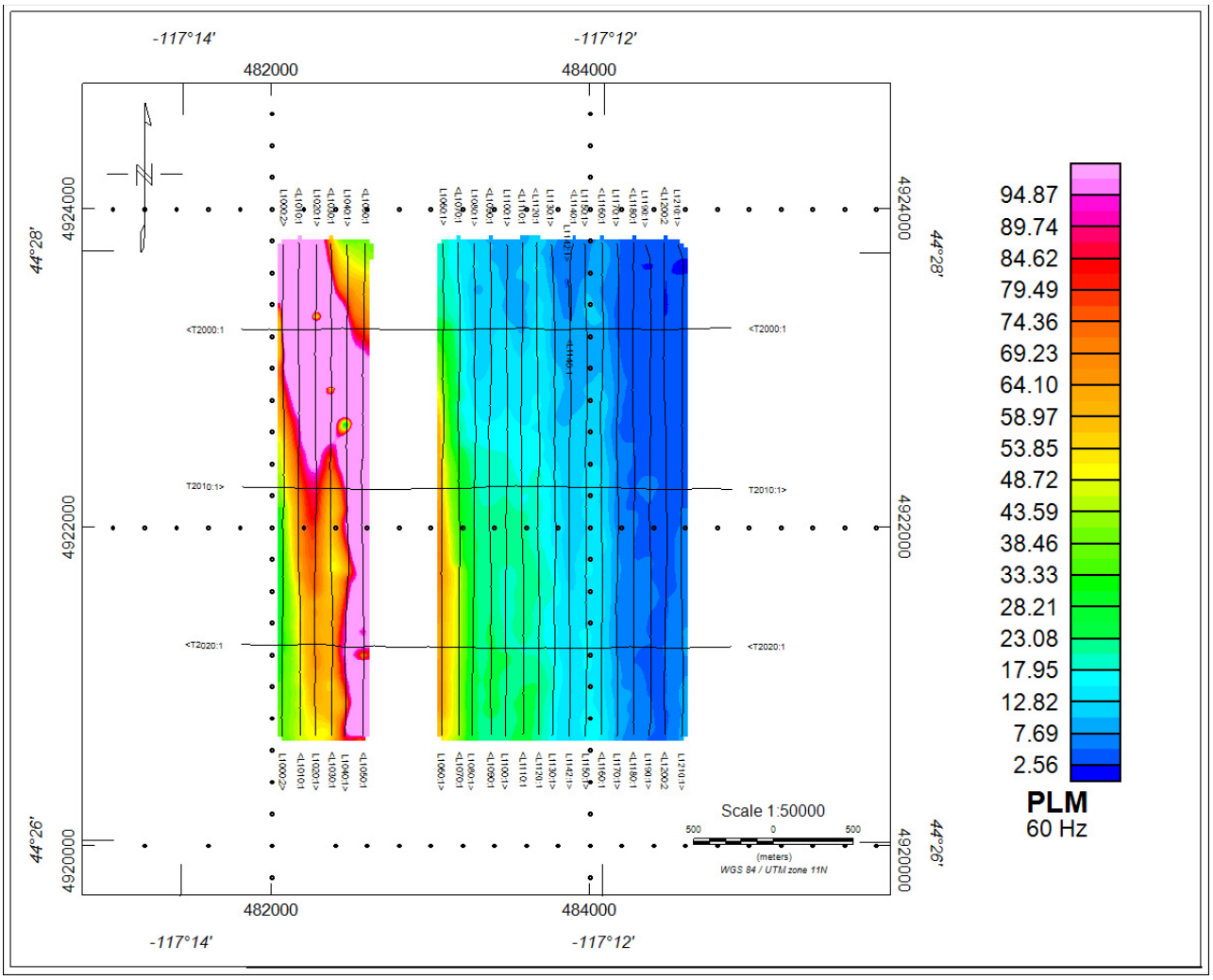

Bayhorse Idaho/Oregon Geophysics Project: Z-component dB/dt Calculated EM Decay Time Constant (Tau) with Calculated Vertical Magnetic Derivative contours




Bayhorse Idaho/Oregon Geophysics Project: Magnetic Tilt-Angle Derivative



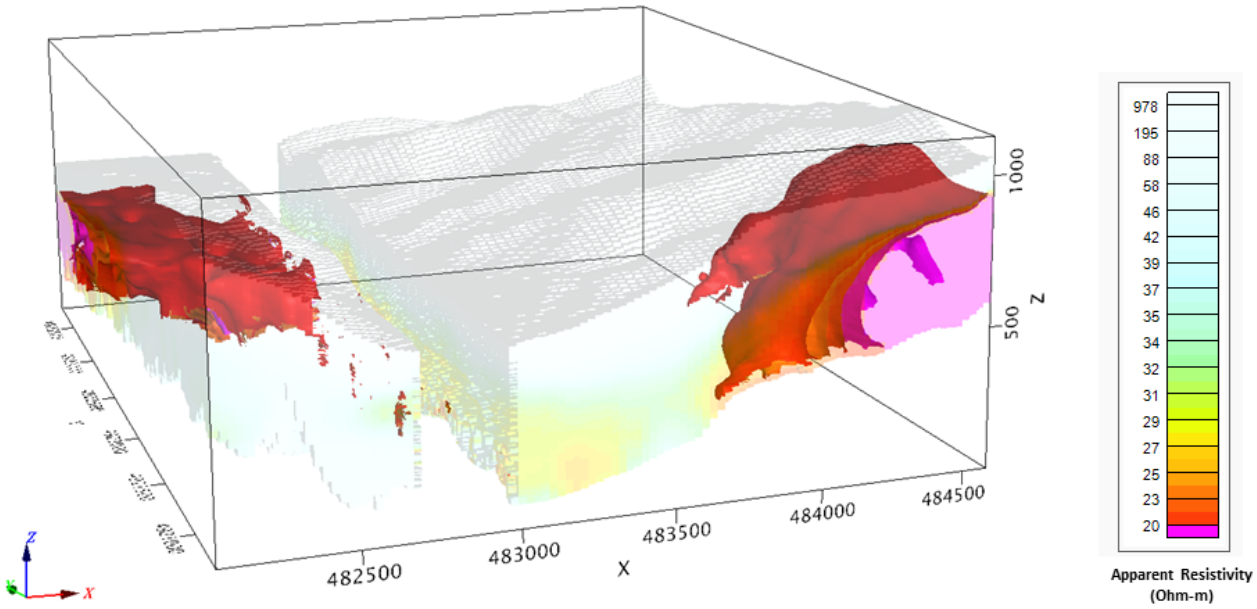

Bayhorse Idaho/Oregon Geophysics Project: Total Magnetic Horizontal Gradient




Bayhorse Idaho/Oregon Geophysics Project: Power Line Monitor (PLM)

# RESISTIVITY DEPTH IMAGE (RDI) MAP

## 3D View of RDI Apparent Resistivity Voxel




WGS 84 / UTM Zone 11N

Bayhorse Silver Inc.
Brownlee Block
Baker City, Oregon, USA
Job Number:GL230249

# APPENDIX D

## GENERALIZED MODELING RESULTS OF THE VTEM SYSTEM

## INTRODUCTION

The VTEM system is based on a concentric or central loop design, whereby, the receiver is positioned at the centre of a transmitter loop that produces a primary field. The wave form is a bi-polar, modified square wave with a turn-on and turn-off at each end.

During turn-on and turn-off, a time varying field is produced (dB/dt) and an electro-motive force (emf) is created as a finite impulse response. A current ring around the transmitter loop moves outward and downward as time progresses. When conductive rocks and mineralization are encountered, a secondary field is created by mutual induction and measured by the receiver at the centre of the transmitter loop.

Efficient modeling of the results can be carried out on regularly shaped geometries, thus yielding close approximations to the parameters of the measured targets. The following is a description of a series of common models made for the purpose of promoting a general understanding of the measured results.

A set of models has been produced for the Geotech VTEM™ system dB/dT Z and X components (see models D1 to D15). The Maxwell™ modeling program (EMIT Technology Pty. Ltd. Midland, WA, AU) used to generate the following responses assumes a resistive half-space. The reader is encouraged to review these models, so as to get a general understanding of the responses as they apply to survey results. While these models do not begin to cover all possibilities, they give a general perspective on the simple and most commonly encountered anomalies.

As the plate dips and departs from the vertical position, the peaks become asymmetrical.

As the dip increases, the aspect ratio (Min/Max) decreases, and this aspect ratio can be used as an empirical guide to dip angles from near 90º to about 30º. The method is not sensitive enough where dips are less than about 30º.

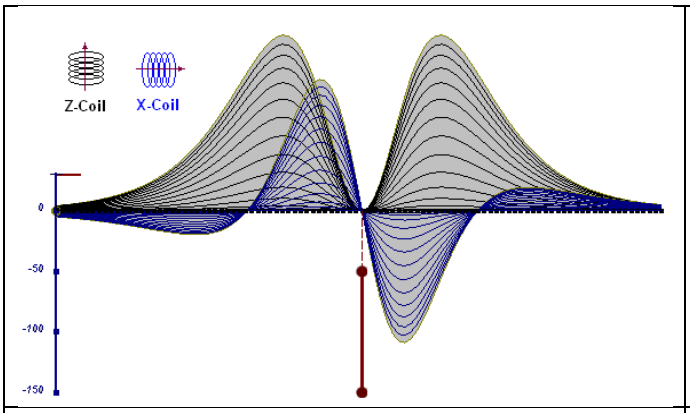



**Figure D-1**: vertical thin plate

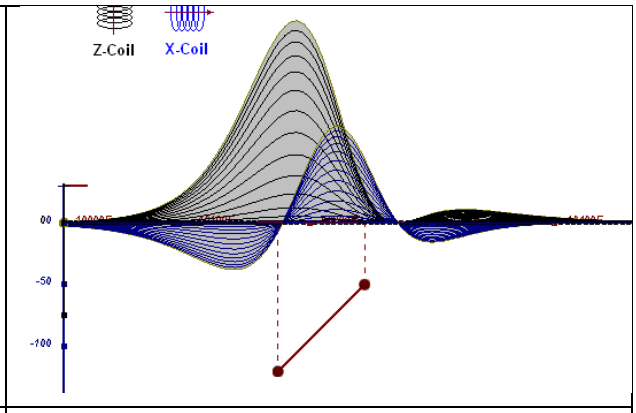



**Figure D-2**: inclined thin plate

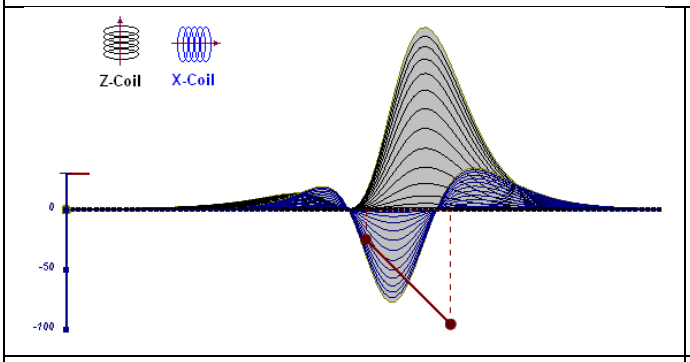



**Figure D-3**: inclined thin plate

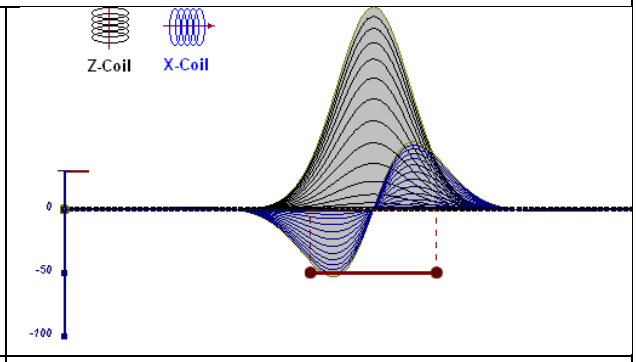



**Figure D-4**: horizontal thin plate

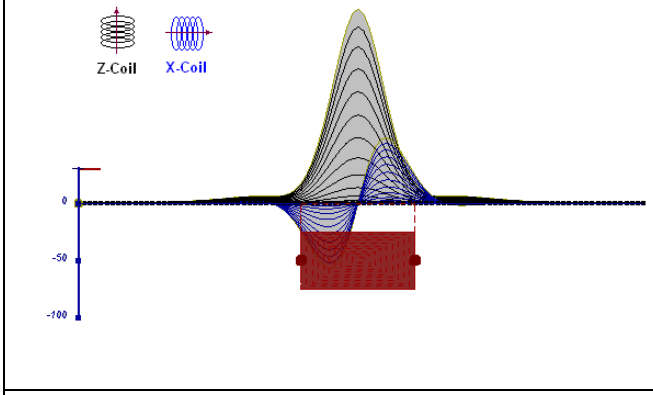



**Figure D-5**: horizontal thick plate (linear scale of the response)

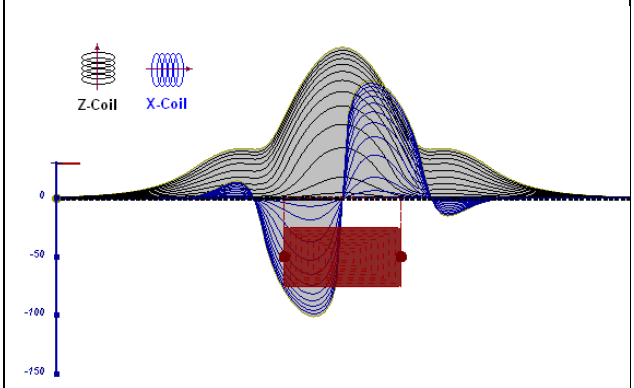



**Figure D-6**: horizontal thick plate (log scale of the response)

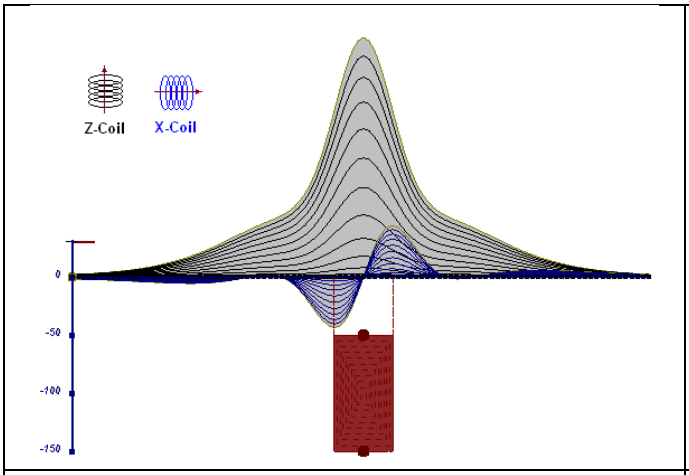



**Figure D-7**: vertical thick plate (linear scale of the response). 50 m depth

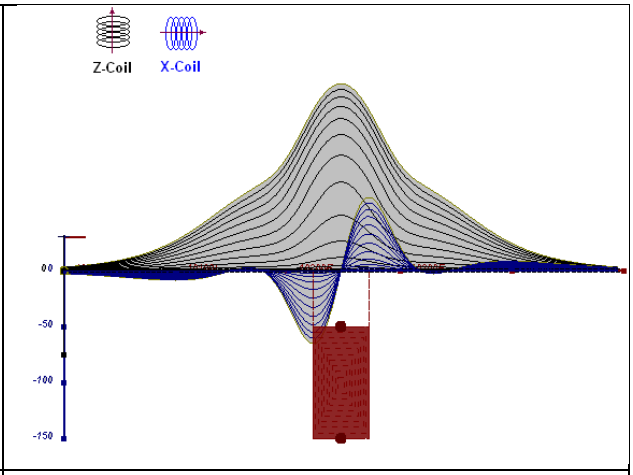



**Figure D-8**: vertical thick plate (log scale of the response). 50 m depth

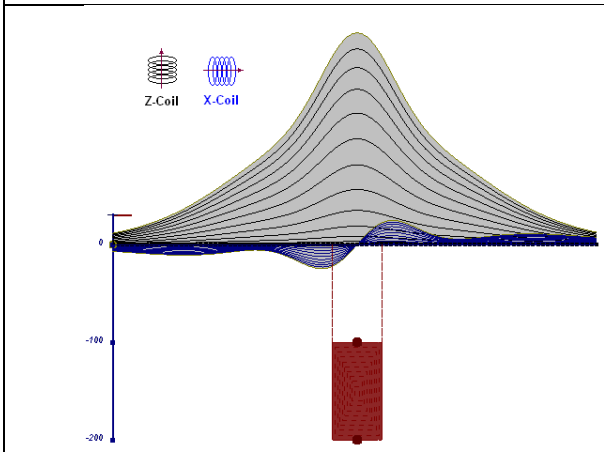



**Figure D-9**: vertical thick plate (linear scale of the response). 100 m depth

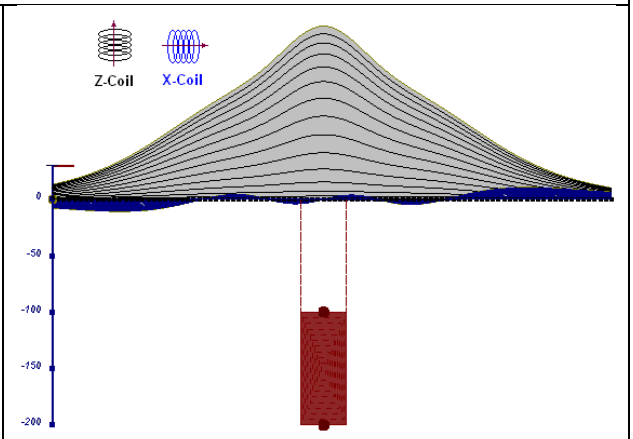



**Figure D-10**: vertical thick plate (linear scale of the response). Depth / horizontal thickness=2.5

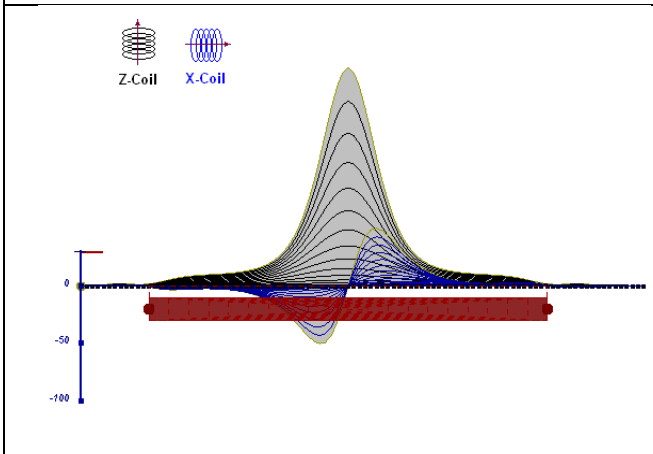



**Figure D-11**: horizontal thick plate (linear scale of the response)

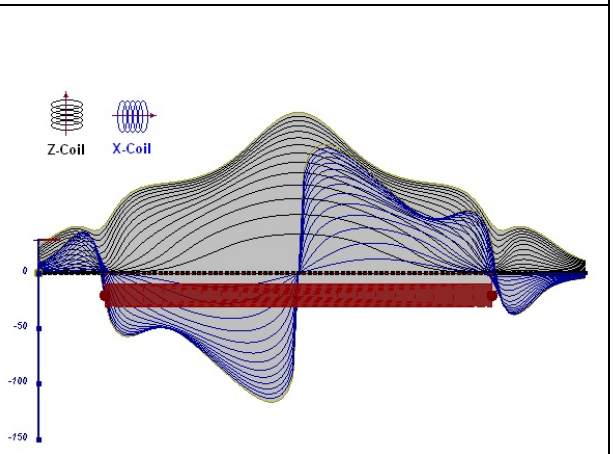



**Figure D-12**: horizontal thick plate (log scale of the response)

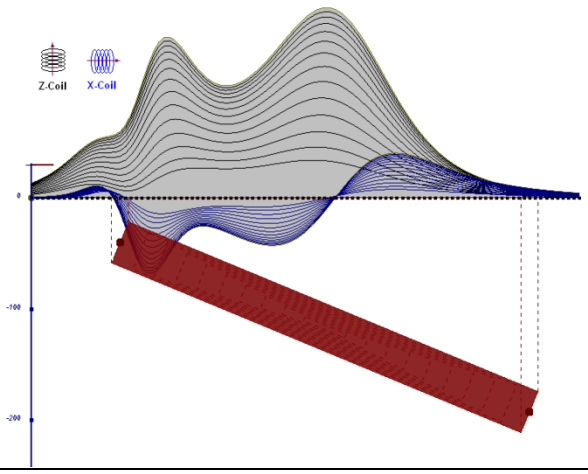



**Figure D-13**: inclined long thick plate

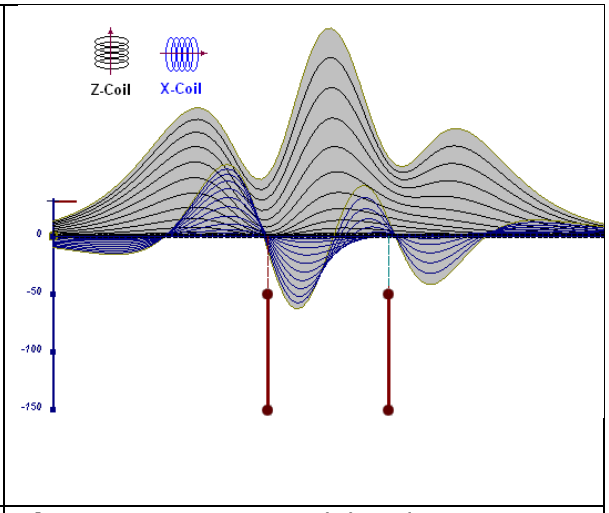



**Figure D-14**: two vertical thin plates

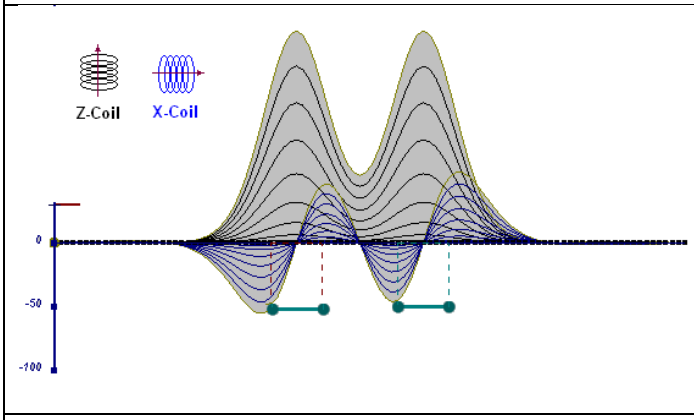



**Figure D-15**: two horizontal thin plates

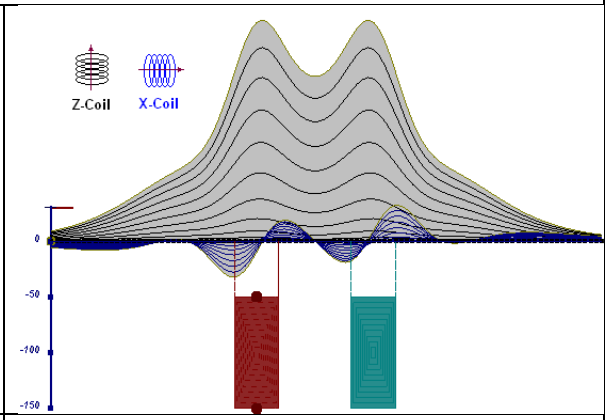



**Figure D-16**: two vertical thick plates

The same type of target but with different thickness, for example, creates different form of the response:

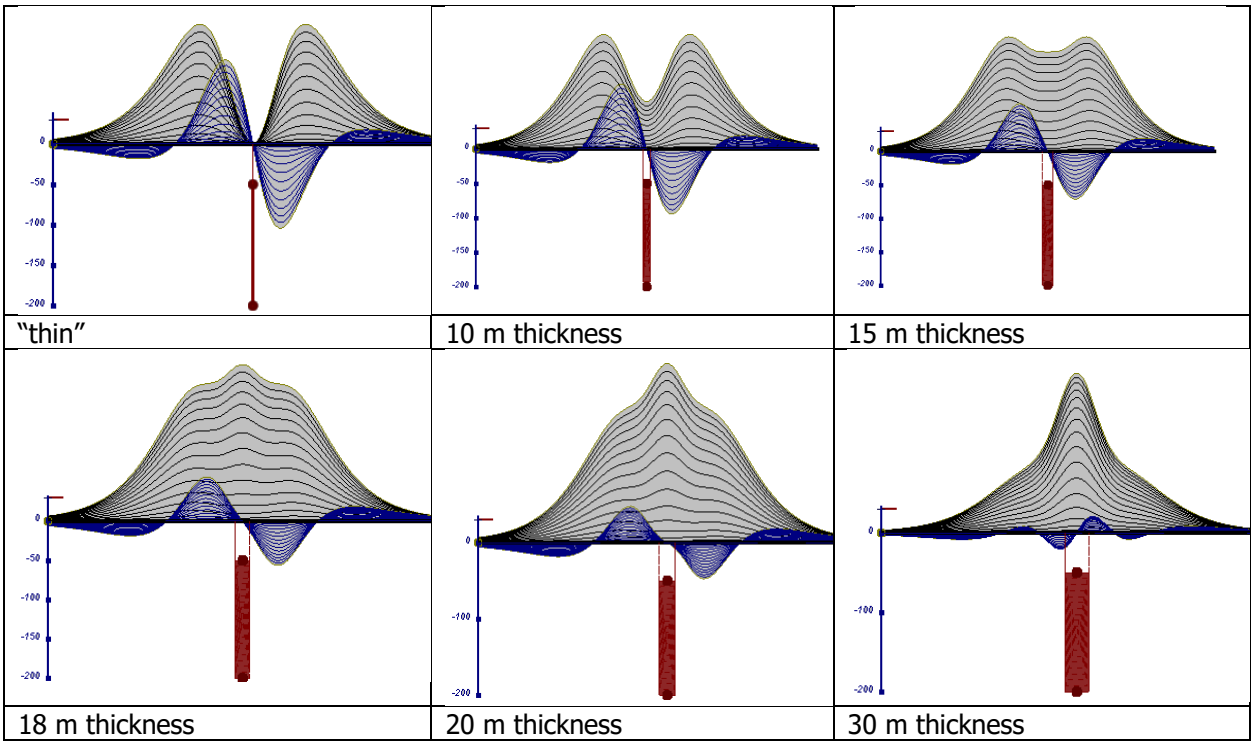



**Figure D-17**: Conductive vertical plate, depth 50 m, strike length 200 m, depth extent 150 m.

**Geotech Ltd.**
September 2010

# APPENDIX E

## EM TIME CONSTANT (TAU) ANALYSIS

Estimation of time constant parameter[1] in transient electromagnetic method is one of the steps toward the extraction of the information about conductance beneath the surface from TEM measurements.

The most reliable method to discriminate or rank conductors from overburden, background or one and other is by calculating the EM field decay time constant (TAU parameter), which directly depends on conductance despite their depth and accordingly amplitude of the response.

## THEORY

As established in electromagnetic theory, the magnitude of the electro-motive force (emf) induced is proportional to the time rate of change of primary magnetic field at the conductor. This emf causes eddy currents to flow in the conductor with a characteristic transient decay, whose Time Constant (Tau) is a function of the conductance of the survey target or conductivity and geometry (including dimensions) of the target. The decaying currents generate a proportional secondary magnetic field, the time rate of change of which is measured by the receiver coil as induced voltage during the Off time.

The receiver coil output voltage ($\mathbf{e_0}$) is proportional to the time rate of change of the secondary magnetic field and has the form,

$$e_0 \alpha (1 / \tau)\, e^{-(t/\tau)}$$

Where,
$\tau$ = L/R is the characteristic time constant of the target (TAU)
R = resistance
L = inductance

From the expression, conductive targets that have small value of resistance and hence large value of $\tau$ yield signals with small initial amplitude that decays relatively slowly with progress of time. Conversely, signals from poorly conducting targets that have large resistance value and small$\tau$, have high initial amplitude but decay rapidly with time[1] (Fig. E1).

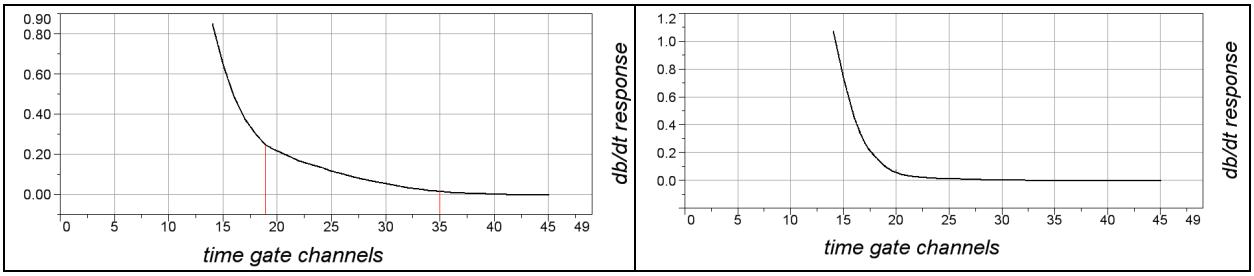



Figure E-1: Left – presence of good conductor, right – poor conductor.

[1] McNeill, JD, 1980, "Applications of Transient Electromagnetic Techniques", Technical Note TN-7 page 5, Geonics Limited, Mississauga, Ontario.

## EM Time Constant (Tau) Calculation

The EM Time-Constant (TAU) is a general measure of the speed of decay of the electromagnetic response and indicates the presence of eddy currents in conductive sources as well as reflecting the "conductance quality" of a source. Although TAU can be calculated using either the measured dB/dt decay or the calculated B-field decay, dB/dt is commonly preferred due to better stability (S/N) relating to signal noise. Generally, TAU calculated on base of early time response reflects both near surface overburden and poor conductors whereas, in the late ranges of time, deep and more conductive sources, respectively. For example, early time TAU distribution in an area that indicates conductive overburden is shown in Figure 2.

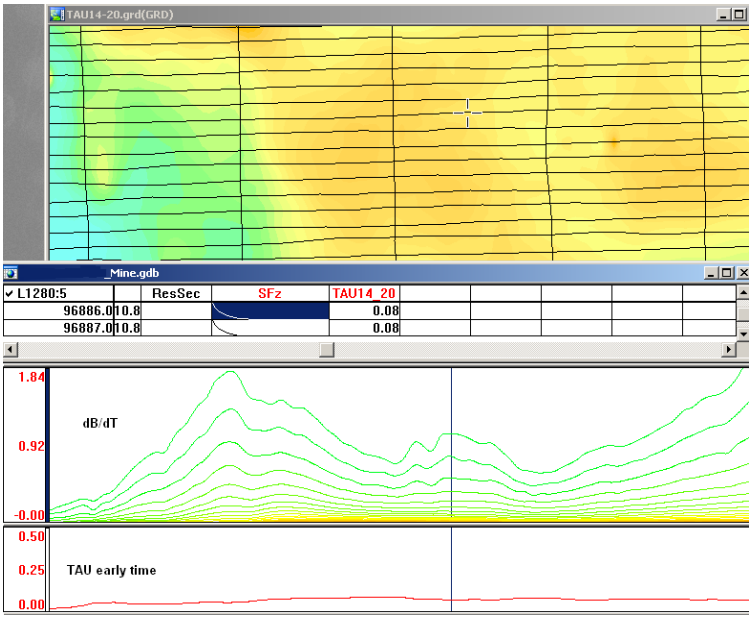



Figure E-2: Map of early time TAU. Area with overburden conductive layer and local sources.

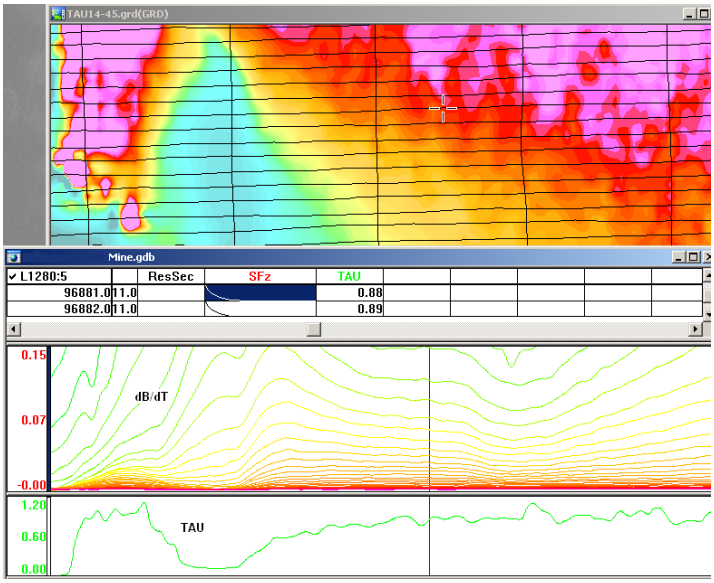



Figure E-3: Map of full time range TAU with EM anomaly due to deep highly conductive target.

There are many advantages of TAU maps:

- TAU depends only on one parameter (conductance) in contrast to response magnitude;
- TAU is integral parameter, which covers time range, and all conductive zones and targets are displayed independently of their depth and conductivity on a single map.
- Very good differential resolution in complex conductive places with many sources with different conductivity.
- Signs of the presence of good conductive targets are amplified and emphasized independently of their depth and level of response accordingly.

In the example shown in Figure 4 and 5, three local targets are defined, each of them with a different depth of burial, as indicated on the resistivity depth image (RDI). All are very good conductors, but the deeper target (number 2) has a relatively weak dB/dt signal yet also features the strongest total TAU (Figure 4). This example highlights the benefit of TAU analysis in terms of an additional target discrimination tool.

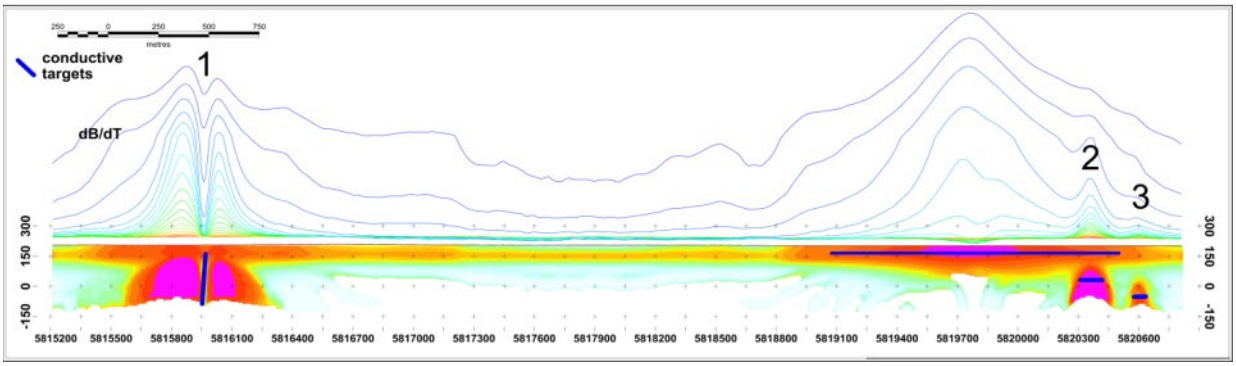



Figure E-4: dB/dt profile and RDI with different depths of targets.

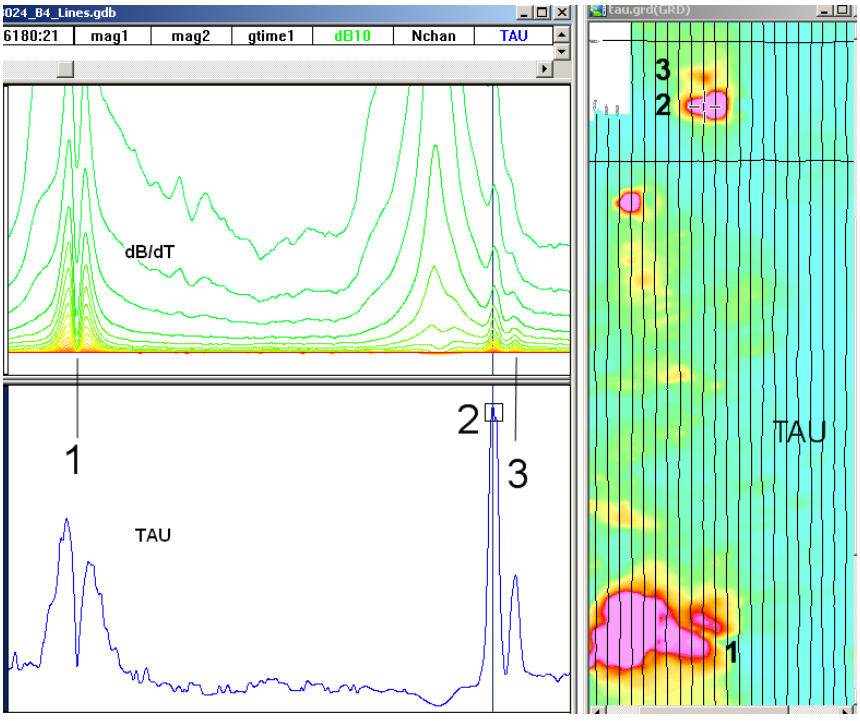



Figure E-5: Map of total TAU and dB/dt profile.

The EM Time Constants for dB/dt and B-field were calculated using the "sliding Tau" in-house program developed at Geotech. The principle of the calculation is based on using of time window (4 time channels) which is sliding along the curve decay and looking for latest time channels which have a response above the level of noise and decay. The EM decays are obtained from all available decay channels, starting at the latest channel. Time constants are taken from a least square fit of a straight-line (log/linear space) over the last 4 gates above a pre-set signal threshold level (Figure E6). Threshold settings are pointed in the "label" property of TAU database channels. The sliding Tau method determines that, as the amplitudes increase, the time-constant is taken at progressively later times in the EM decay. Conversely, as the amplitudes decrease, Tau is taken at progressively earlier times in the decay. If the maximum signal amplitude falls below the threshold or becomes negative for any of the 4 time gates, then Tau is not calculated and is assigned a value of "dummy" by default.

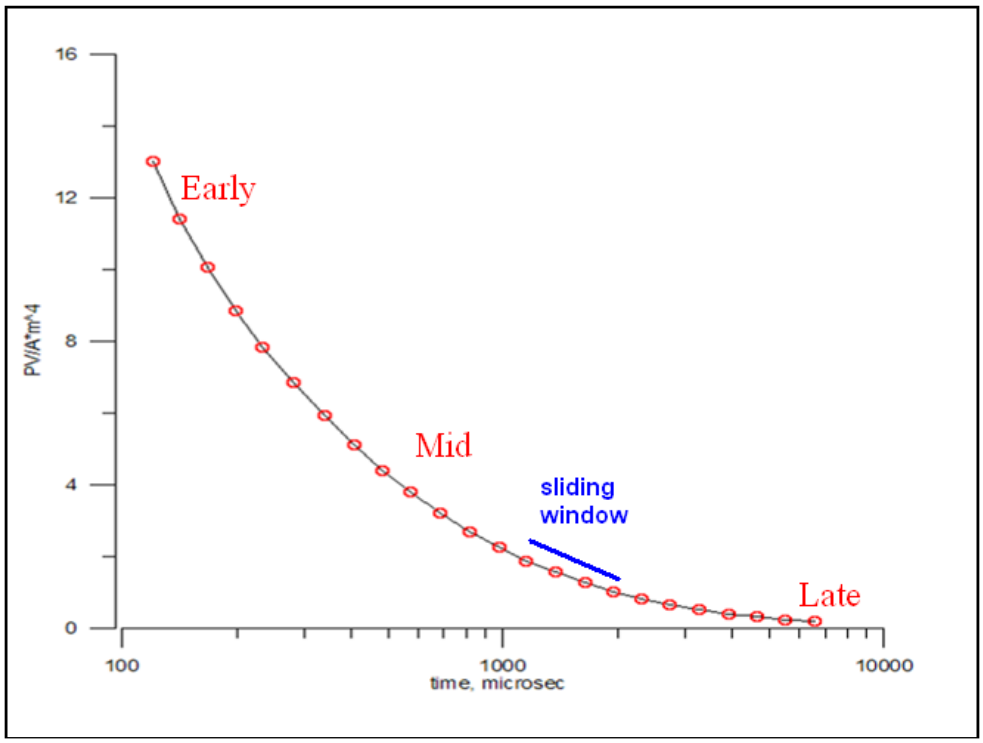



Figure E-6: Schematic VTEM dB Z /dt decay showing Geotech sliding-Tau method for calculating TAU.

**Geotech Ltd.**
September 2010

# APPENDIX F

## TEM RESISTIVITY DEPTH IMAGING (RDI)

Resistivity depth imaging (RDI) is technique used to rapidly convert EM profile decay data into an equivalent resistivity versus depth cross-section, by deconvolving the measured TEM data.

The RDI algorithm for Resistivity-Depth Imaging is based on scheme of the apparent resistivity transform by Meju (1998)[1] for the TEM response in a conductive half-space. The program was developed by Geotech Ltd. and depth calibrated based on forward plate modeling for VTEM system configuration (Fig. 1-10).

RDIs provide reasonable indications of conductor relative depth and vertical extent, as well as accurate 1D layered-earth apparent conductivity/resistivity structure across VTEM flight lines. Approximate depth of investigation of a TEM system, image of secondary field distribution in half space, effective resistivity, initial geometry and position of conductive targets is the information obtained on base of the RDIs.

Maxwell EM plate forward modeling with RDI sections from the synthetic responses (VTEM system) are presented below.

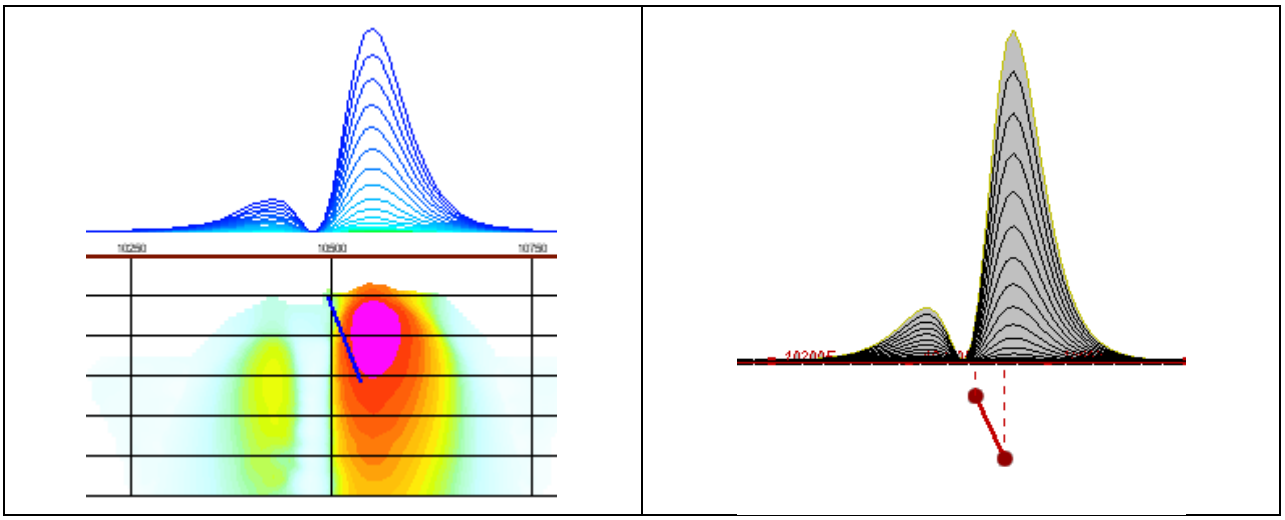


Figure F-1: Maxwell plate model and RDI from the calculated response for conductive "thin" plate (depth 50 m, dip 65 degree, depth extent 100 m).

[1] Meju,M.A., 1998, Short Note: A simple method of transient electromagnetic data analysis, Geophysics, **63**, 405–410.

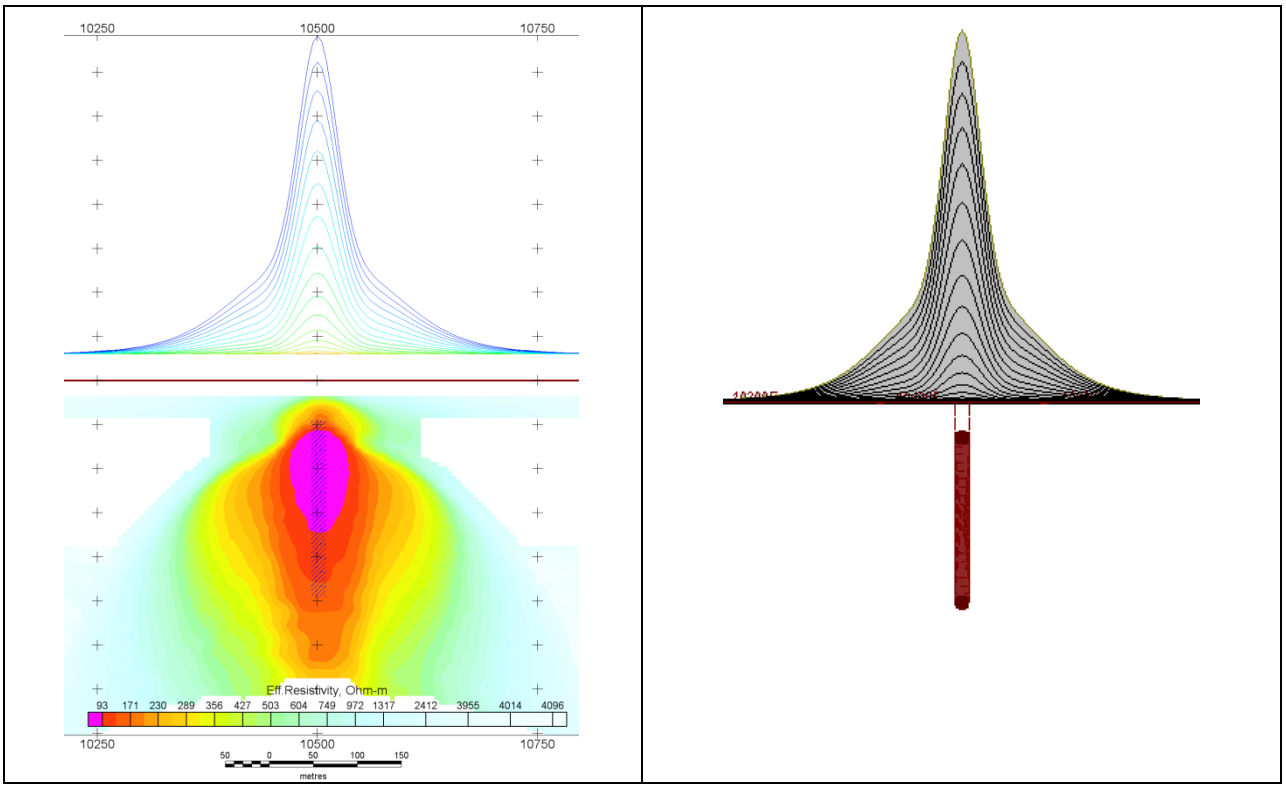



Figure F-2: Maxwell plate model and RDI from the calculated response for "thick" plate 18 m thickness, depth 50 m, depth extent 200 m).

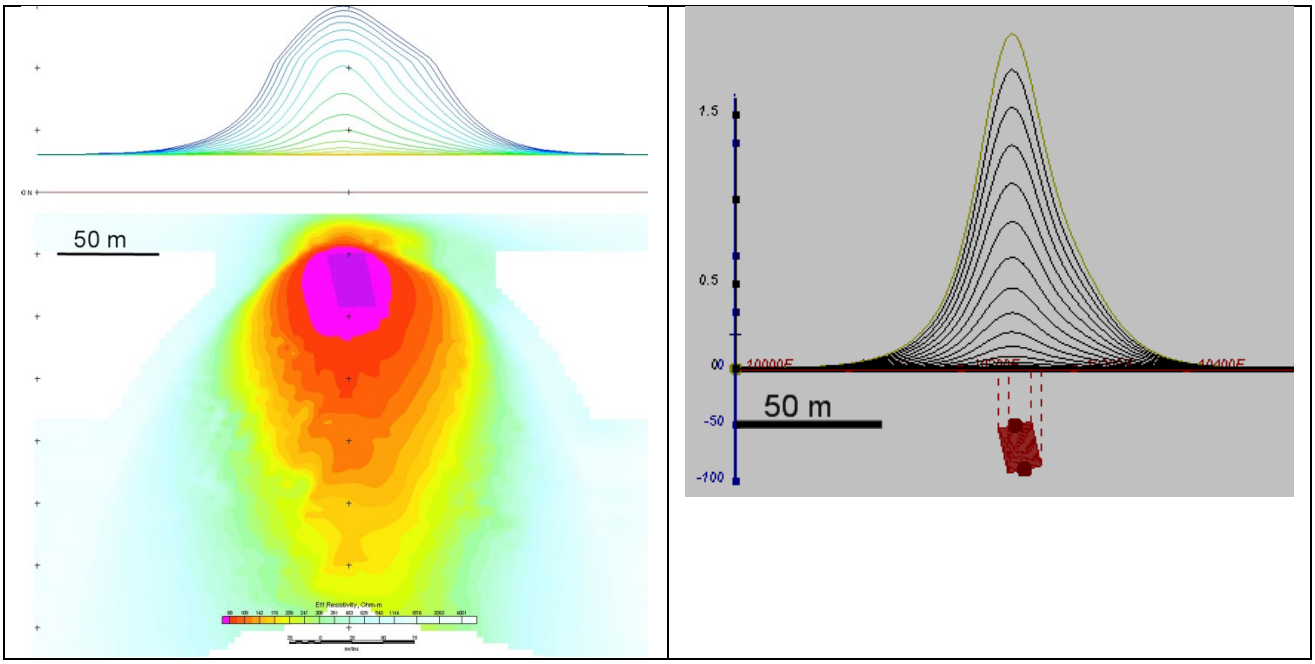



Figure F-3: Maxwell plate model and RDI from the calculated response for bulk ("thick") 100 m length, 40 m depth extent, 30 m thickness

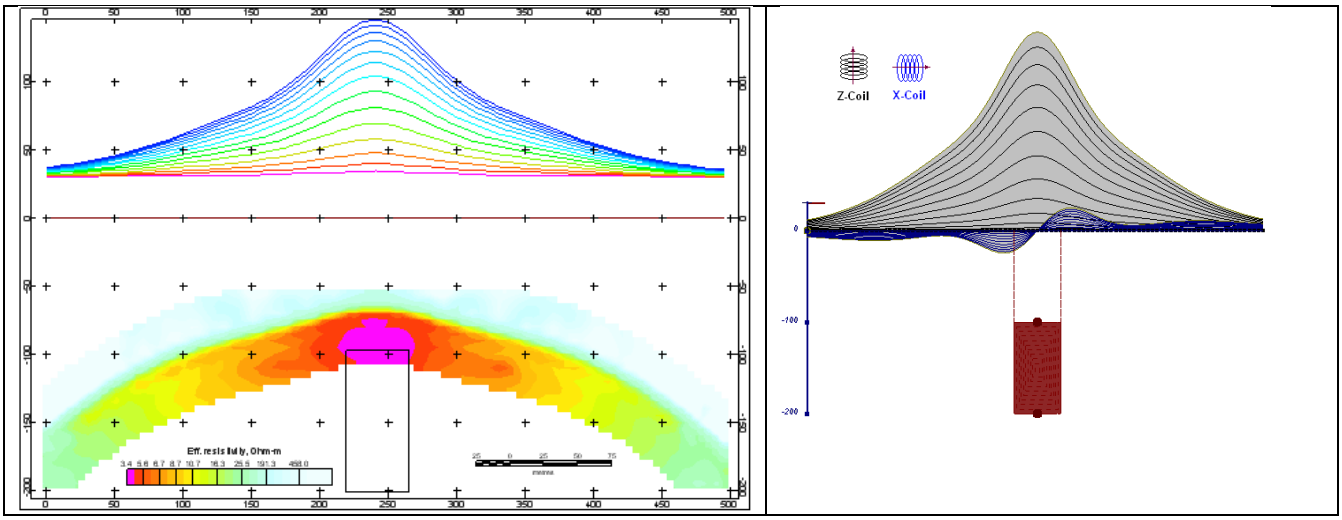



Figure F-4: Maxwell plate model and RDI from the calculated response for "thick" vertical target (depth 100 m, depth extent 100 m). 19-44 chan.

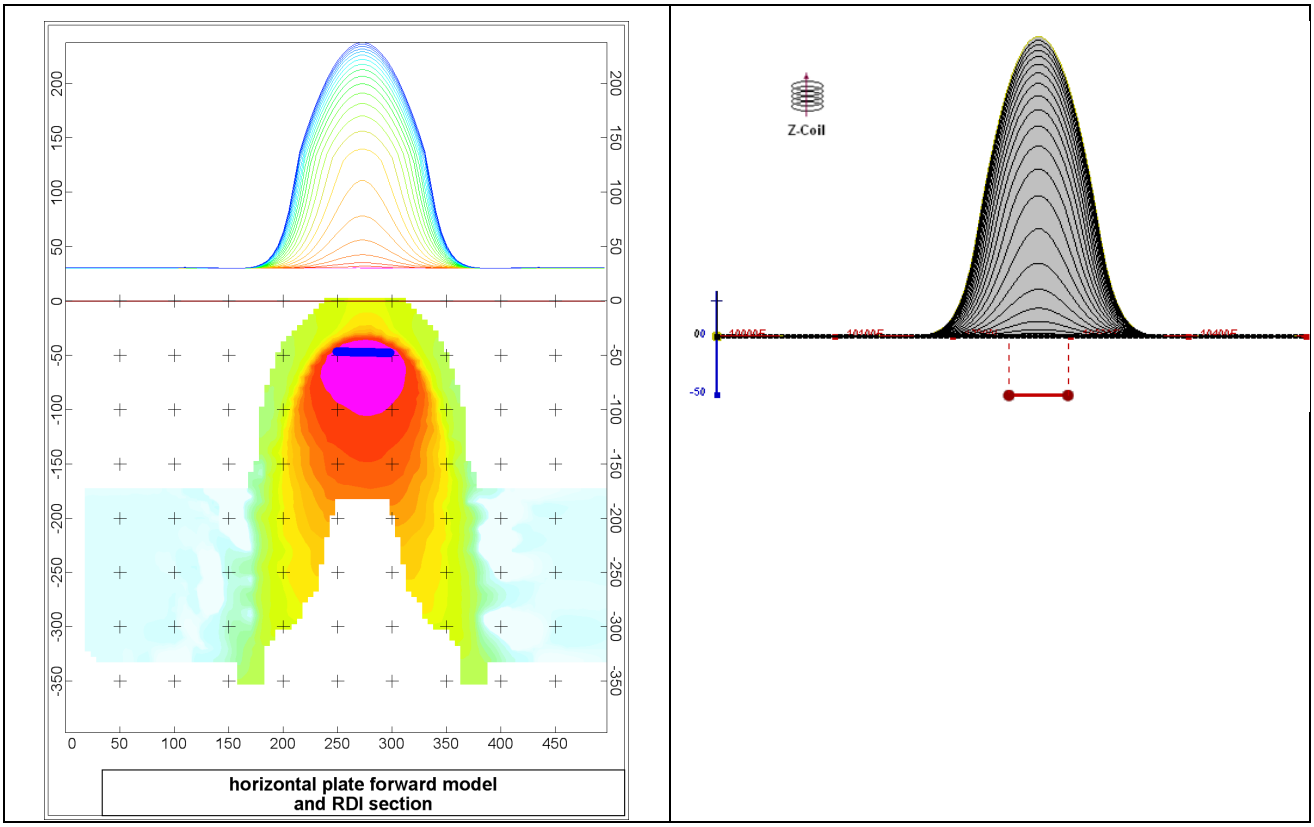



Figure F-5: Maxwell plate model and RDI from the calculated response for horizontal thin plate (depth 50 m, dim 50x100 m). 15-44 chan.

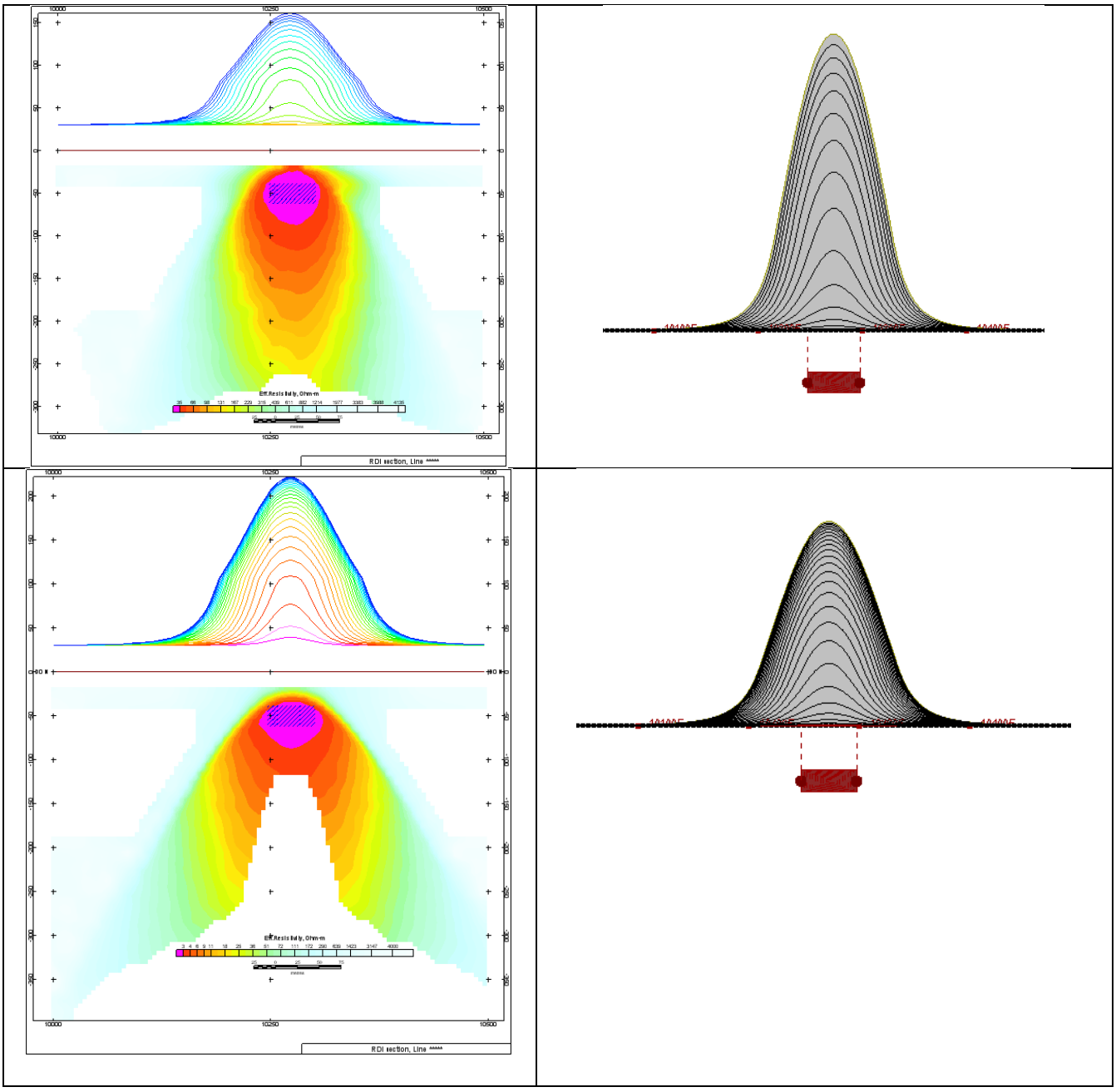


Figure F-6: Maxwell plate model and RDI from the calculated response for horizontal thick (20m) plate – less conductive (on the top), more conductive (below).

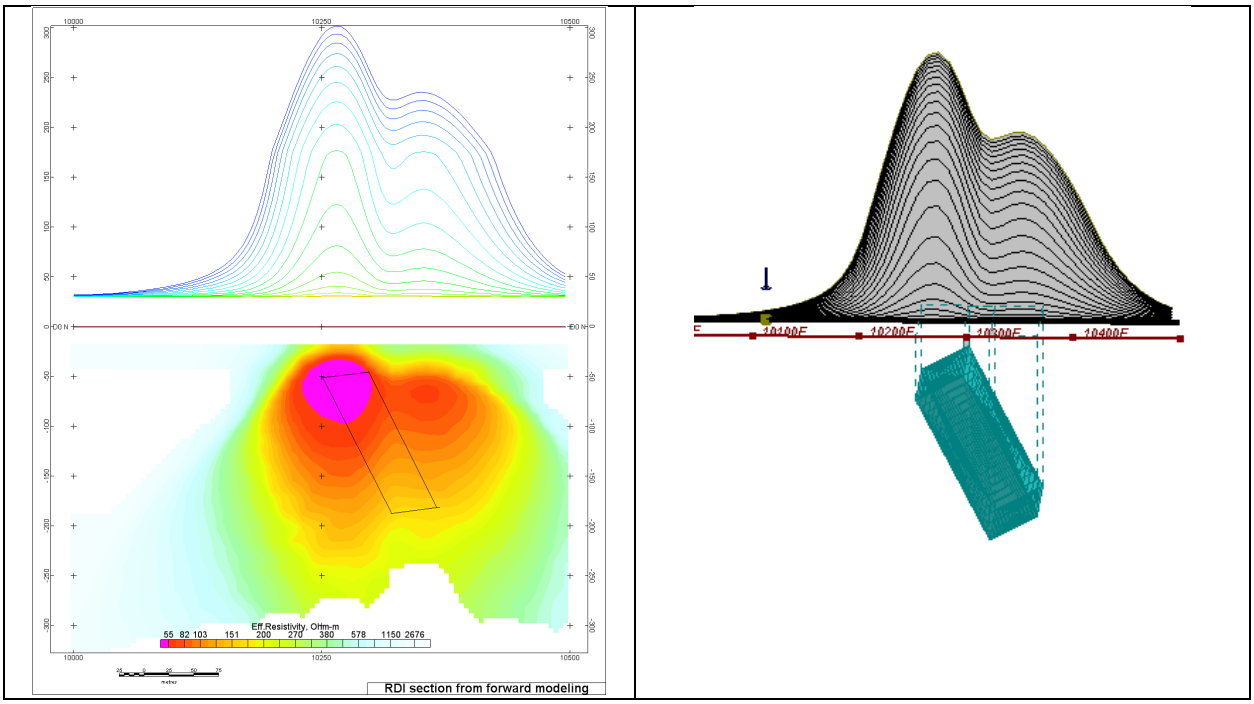



Figure F-7: Maxwell plate model and RDI from the calculated response for inclined thick (50m) plate. Depth extent 150 m, depth to the target 50 m.

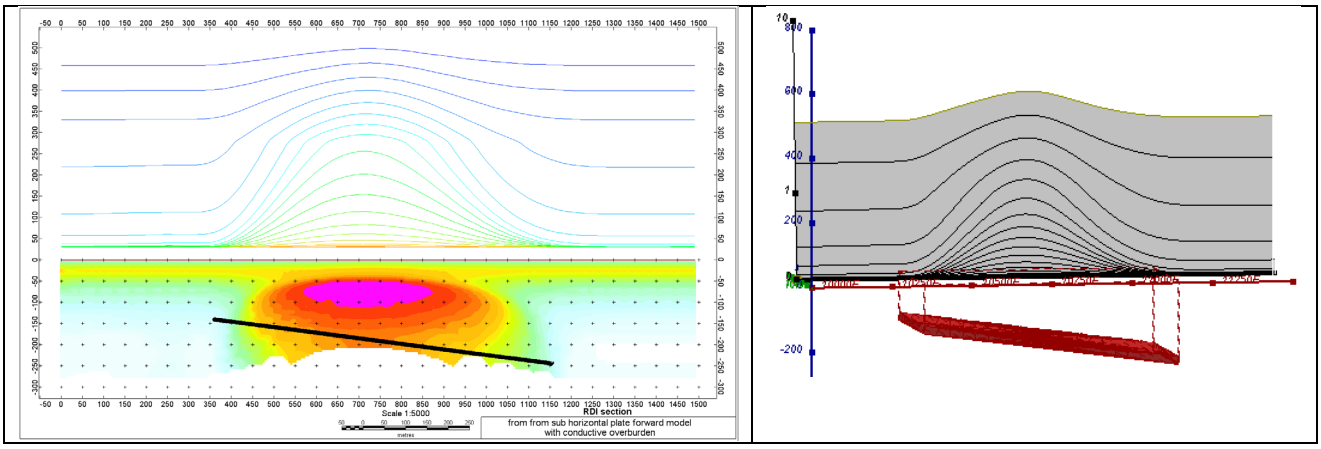



Figure F-8: Maxwell plate model and RDI from the calculated response for the long, wide and deep subhorizontal plate (depth 140 m, dim 25x500x800 m) with conductive overburden.

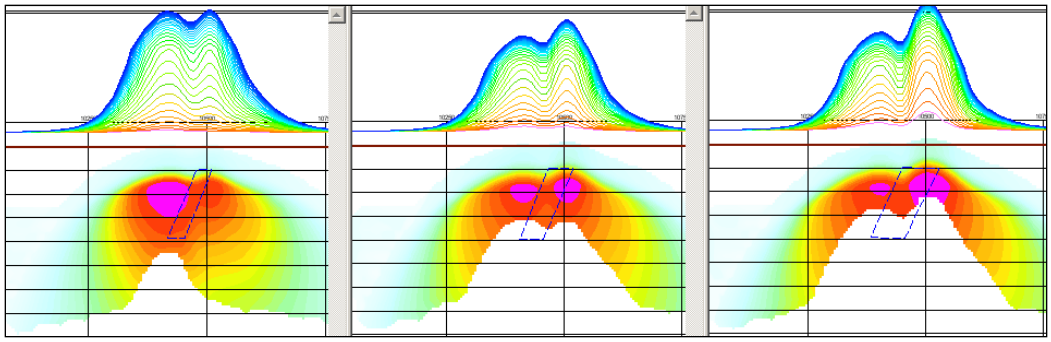


Figure F-9: Maxwell plate models and RDIs from the calculated response for "thick" dipping plates (35, 50, 75 m thickness), depth 50 m, conductivity 2.5 S/m.

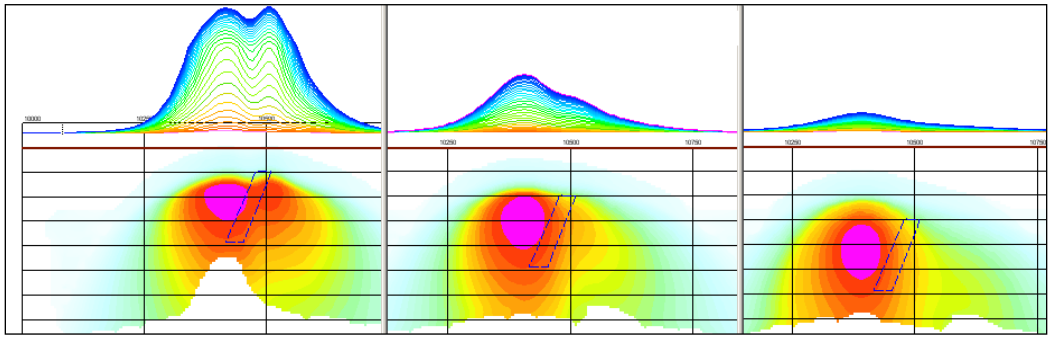


Figure F-10: Maxwell plate models and RDIs from the calculated response for "thick" (35 m thickness) dipping plate on different depth (50, 100, 150 m), conductivity 2.5 S/m.

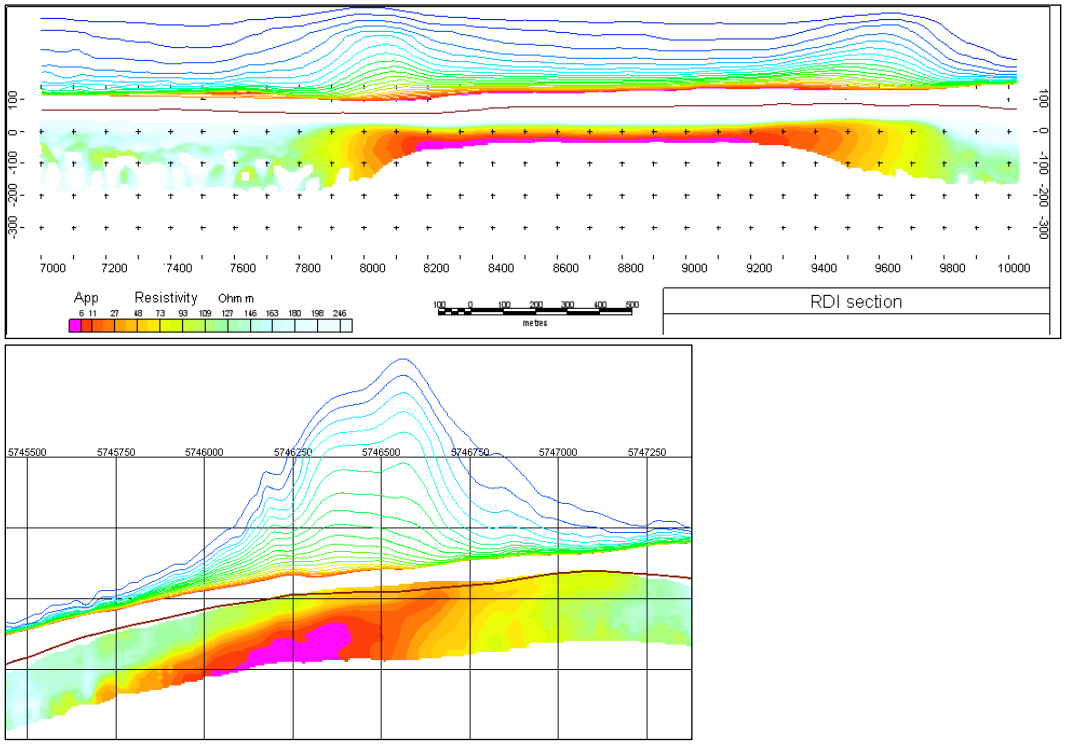
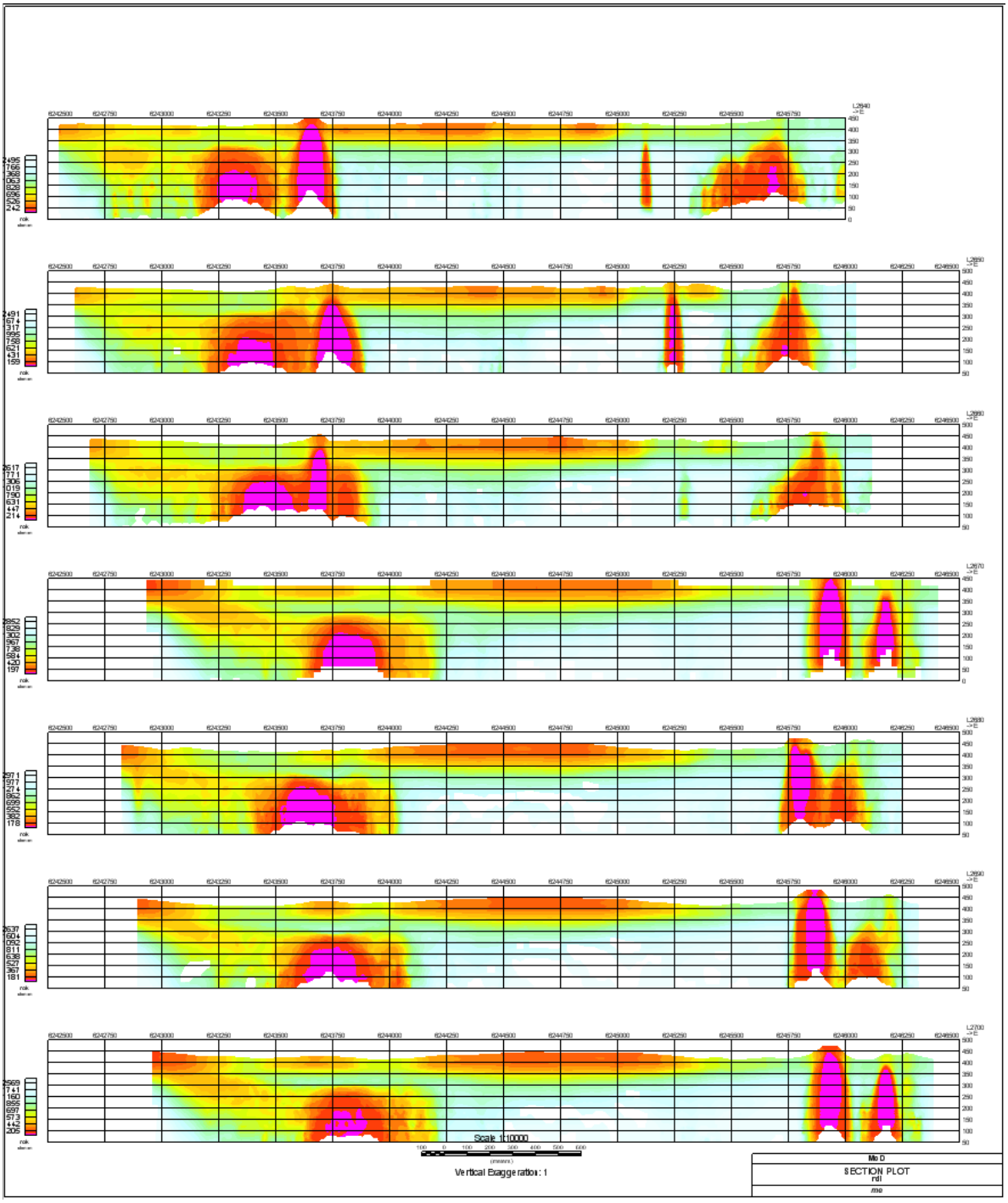


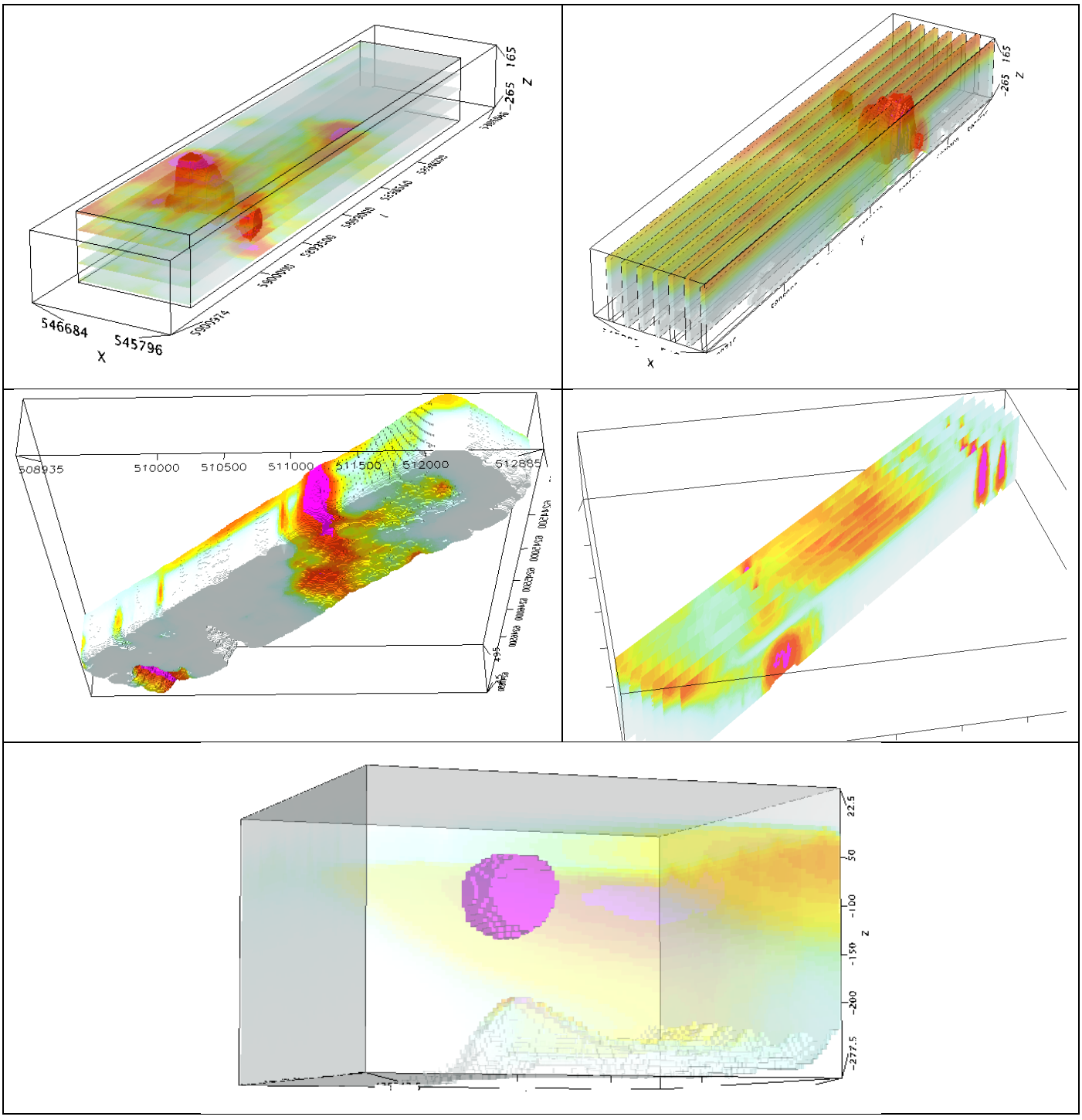

Figure F-11: RDI section for the real horizontal and slightly dipping conductive layers.

# FORMS OF RDI PRESENTATION

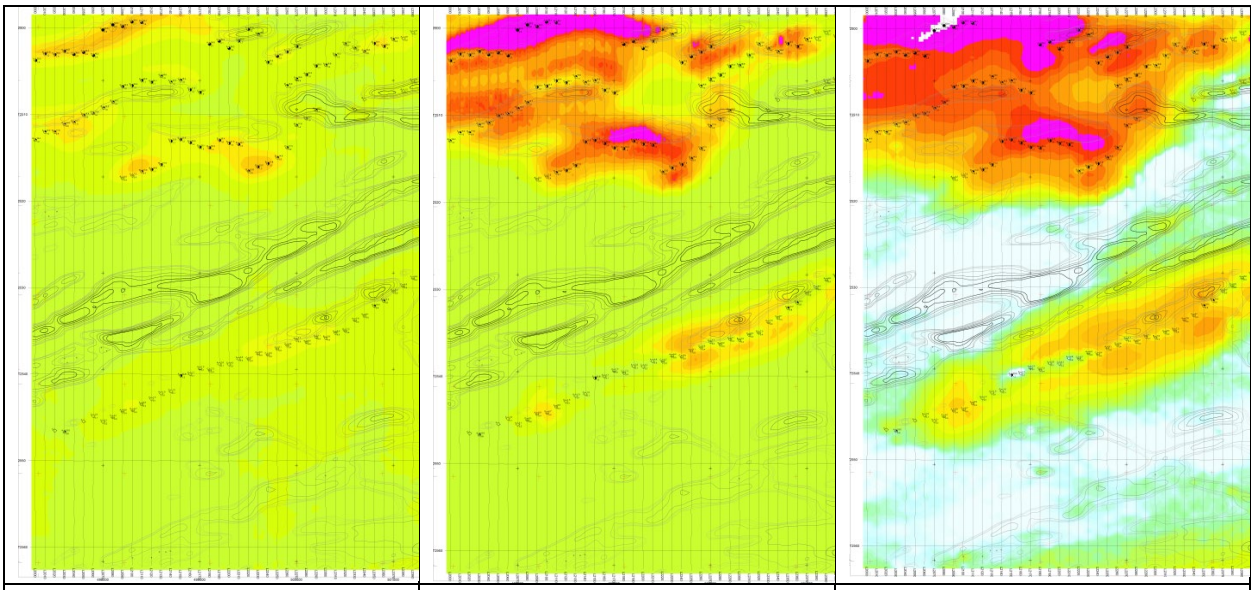
## PRESENTATION OF SERIES OF LINES



## 3D PRESENTATION OF RDIS

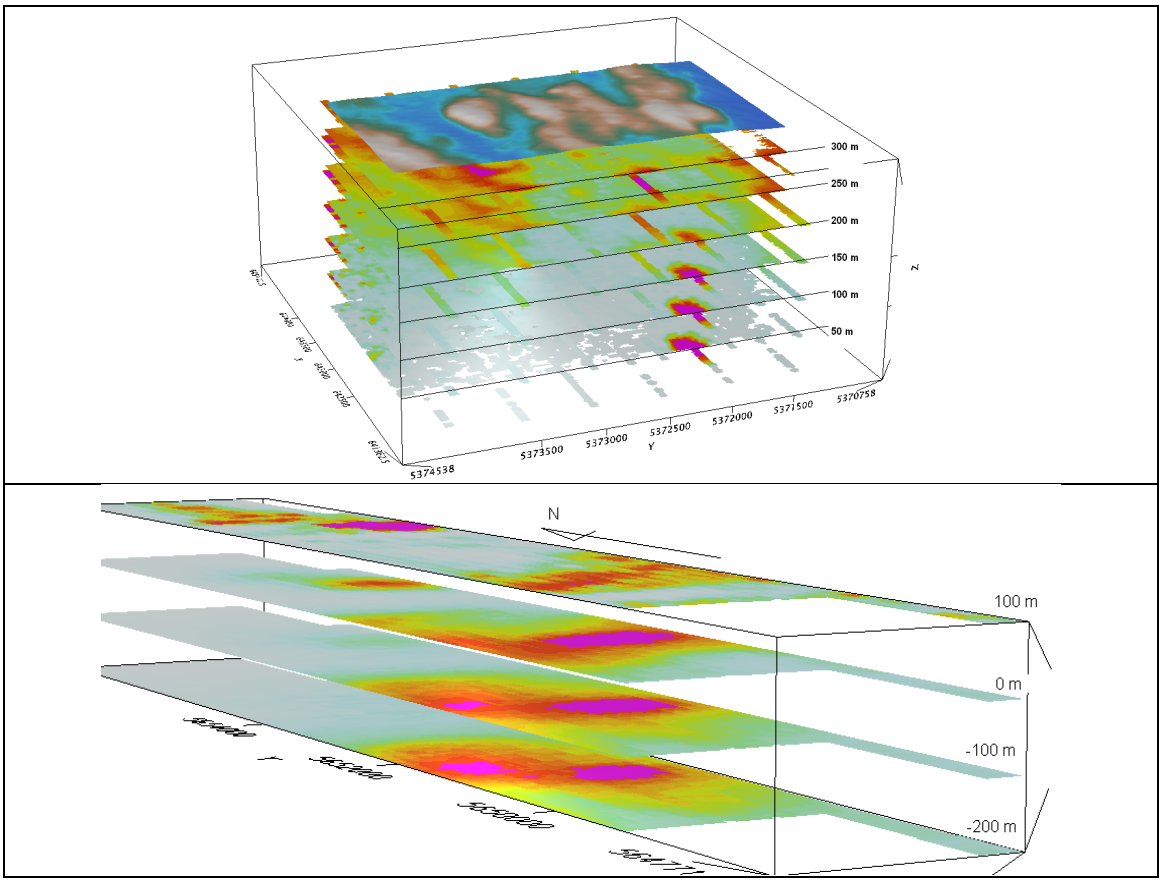


## APPARENT RESISTIVITY DEPTH SLICES PLANS:



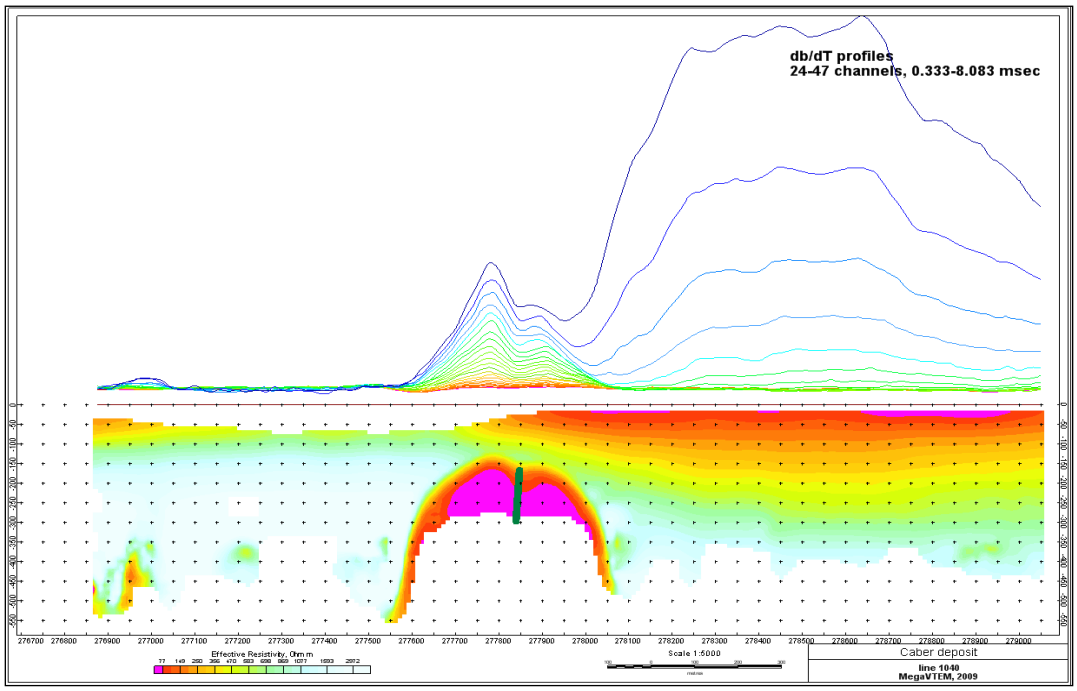
| 0 m (surface) | -100 m | -200 m |
|---|---|---|

## 3D VIEWS OF APPARENT RESISTIVITY DEPTH SLICES:

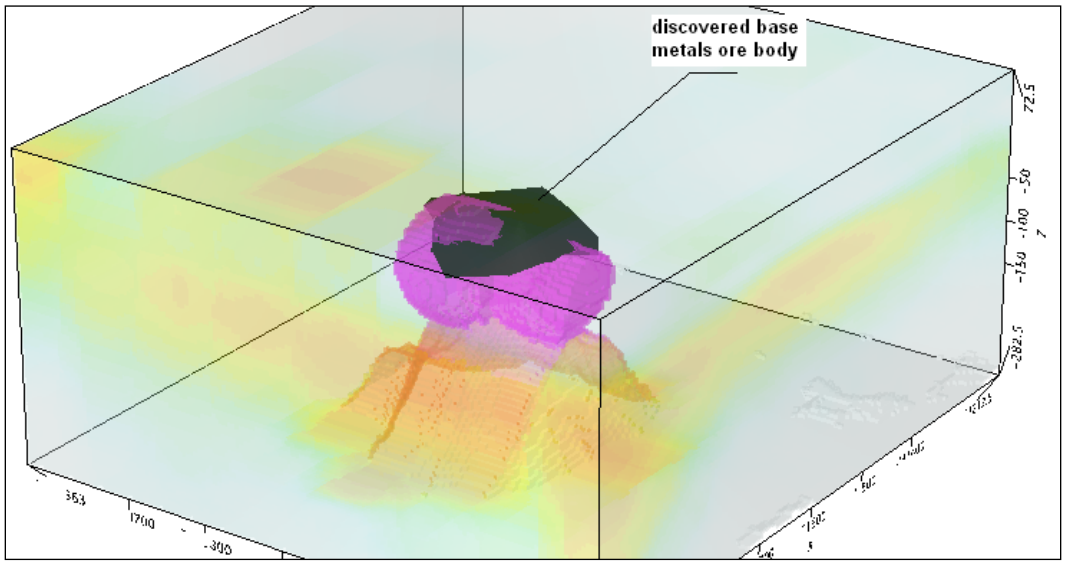


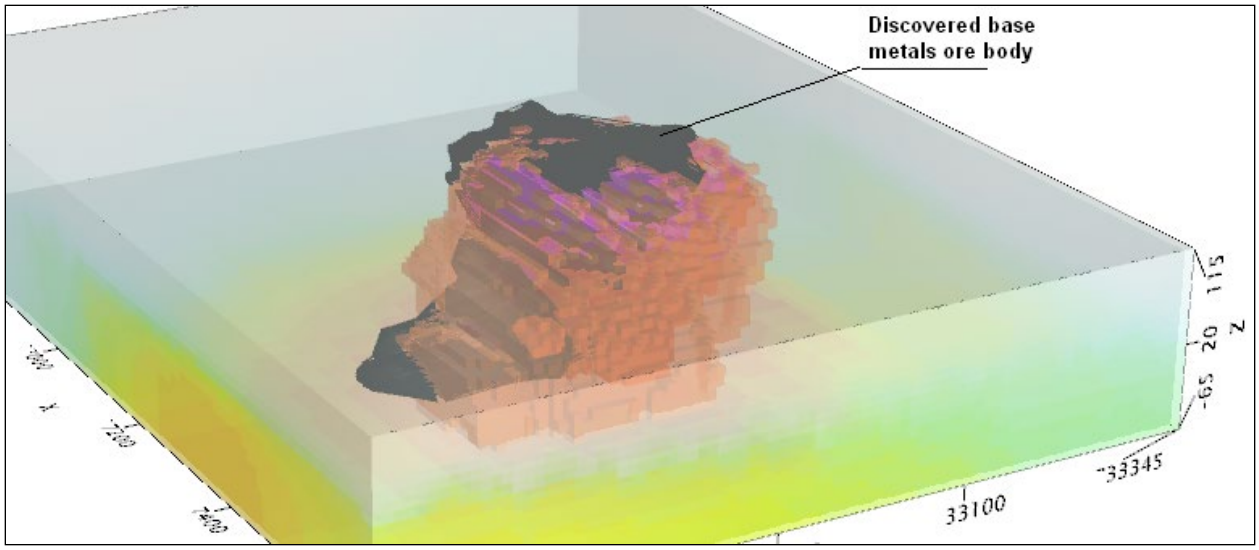
## REAL BASE METAL TARGETS IN COMPARISON WITH RDIS:

RDI section of the line over Caber deposit ("thin" subvertical plate target and conductive overburden.




## 3D RDI VOXELS WITH BASE METALS ORE BODIES (MIDDLE EAST):






**Geotech Ltd.**
April 2011

# APPENDIX G
## RESISTIVITY DEPTH IMAGES (RDI)

Please see RDI Folder on DVD for the PDF's